DYNAMIC ANALYSIS OF ELEVATOR IN-CAR VIBRATIONS AND RIDE QUALITY USING MESHLESS METHOD

Lappeenranta–Lahti University of Technology LUT

Master's thesis in Mechanical Engineering

2022

Jussi Leppänen

Examiners: Professor Jussi Sopanen

D. Sc. (Tech.) Eerik Sikanen

ABSTRACT

Lappeenranta–Lahti University of Technology LUT

LUT School of Energy Systems

Mechanical Engineering

Jussi Leppänen

Dynamic Analysis of the Elevator in-car Vibrations and Ride Quality Using Meshless Method

Master's thesis

2022

96 pages, 41 figures, 13 tables and 1 appendix

Examiners: Professor Jussi Sopanen and D.Sc. (Tech.) Eerik Sikanen

Supervisors: D.Sc. (Tech.) Gabriela Roivainen and M.Sc. (Tech.) Tarvo Viita-aho

Keywords: Elevator, Elevator Ride Quality, Dynamic Analysis, Harmonic Response Analysis, Forced Response, Structural Dynamics, Meshless Method, Meshfree Method, Finite Element Method, Simulation.

This thesis aimed to perform dynamic analysis of the elevator car system including car frame and doors. The dynamic analysis results were examined and utilized for nominating potential design changes for improving the ride quality of the elevator car. The dynamic analysis results were validated by performing measurements of in-car physical movements during the elevator run. The in-car movements were measured with an EVA measurement instrument used for the elevator ride quality assessment. The dynamic analyses were performed with a meshless method. This method offers the possibility of obtaining structural analysis results quicker than traditional element methods from the 3D models of the analyzed structure assemblies. The theory of finite element methods and meshfree methods are discussed in this thesis. Additionally, a benchmarking was done for the SimSolid analysis software used in the case studies. The benchmarking showed that the results of the dynamic analysis done by SimSolid could be compared to the traditionally used mesh-based methods like those used in FEMAP.

TIIVISTELMÄ

Lappeenrannan–Lahden teknillinen yliopisto LUT

LUT Energiajärjestelmät

Konetekniikka

Jussi Leppänen

Hissikorin dynamiikan sekä ajomukavuuden analysointi verkottomalla menetelmällä

Konetekniikan diplomityö

2022

96 sivua, 41 kuvaa, 13 taulukkoa ja 1 liite

Tarkastajat: Professori Jussi Sopanen ja TkT Eerik Sikanen

Ohjaajat: TkT Gabriela Roivainen ja DI Tarvo Viita-aho

Avainsanat: hissi, ajomukavuus, dynamiikka, dynamiikan laskenta, harmoninen vaste, pakkovärähtely, rakenteiden dynamiikka, verkoton elementtimenetelmä, elementtimenetelmä, simulointi.

Tämän diplomityön tavoitteena on suorittaa dynamiikan laskenta hissikorikokoonpanolle, johon kuuluu korin lisäksi korikehys ja korinovet. Laskennan tuloksia analysoidaan, jonka myötä pyritään löytämään mahdollisia parannusehdotuksia hissikorin ajomukavuudelle. Laskennan tuloksia on validoitu mittaamalla hissikorin liikkeitä hissin ajon aikana. Hissikorin liikkeitä on mitattu EVA-mittainstrumentilla, jota käytetään yleisesti hissikorin ajomukavuuden arviointiin. Dynamiikan laskenta on suoritettu verkottomalla menetelmällä. Kyseinen menetelmä tarjoaa mahdollisuuden suorittaa rakenteen dynamiikan laskentaa nopeammin kuin yleisesti käytössä olevat verkolliset elementtimenetelmät. Tässä DI-työssä on esitelty verkottoman sekä tavallisen elementtimenetelmän teoria. Lisäksi työ sisältää dynaamisen laskennan vertailun SimSolidin verkottoman elementtimenetelmän sekä FEMAPin verkollisen elementtimenetelmän välillä.

ACKNOWLEDGEMENTS

I would like to take this opportunity to show gratitude towards my examiners and supervisors for this thesis. I have all the support and guidance that I need from my examiners, supervisors and colleagues thorough the writing of this thesis.

I would like to express my gratitude to Gabriela Roivainen D.Sc. (Tech.) and Tarvo Viitaaho M.Sc. (Tech.) for providing me with an opportunity to write this thesis, all the guidance to be successful and sharing your vast experience. Thank you also for motivating and supporting me to learn new professional skills.

I would also want to show my gratitude towards Professor Jussi Sopanen and Eerik Sikanen D. Sc (Tech.) for the valuable guidance, support and suggestions for my thesis. Your advicess and constructive feedback enhanced my learning.

Finally, I would like to thank my parents and family for all the support.

Leppänen Jussi Matti,

Hyvinkää 10.01.2022

SYMBOLS AND ABBREVIATIONS

Roman characters

A	weight moment matrix	
A	area	$[m^2]$
B	strain displacement matrix	
D	diameter	[m]
F	force	[N]
I	second moment of inertia	$[m^4]$
f	frequency	[Hz]
k	stiffness coefficient	
K	stiffnes matrix	
l	Length of the element	
M	mass matrix	
N	matrix of shape functions	
N	normal axial force	[N]
O	amplitude	
S	shape function	
u	interpolation function	
U	vector of field variables	
u	eigenvector	
v	Speed	[m/s]
x	displacement in x-direction	
X	field variable	

Greek characters

$\boldsymbol{\Phi}$	vector of shape functions
Ω	element domain
ω	natural frequency
λ	natural frequency parameter

Subscripts

b	bar element
be	beam element
e	element
n	nominal speed
nb	natural frequency of the beam
np	natural frequency of the plate
rb	rigid body mode
rg	roller guides
rp	ropes
sys	system

Abbreviations

BTF	Back-To-Front
DBG	Distance Between Guides
DOF	Degree of Freedom
EFG	Element-free Galerkin

FEA	Finite Element Analysis
FEM	Finite Element Method
FFT	Fast Fourier Transform
MDOF	Multi Degrees of Freedom
MR	Elevator with Machine Room
MRL	Machine room-less elevators

Table of contents

1. Introduction

Elevator manufacturers have many goals that are increasingly driven by sustainability. Typically, these goals leads to designs of systems that are lighter having fewer components and are easier to install and transport. Making elevator components lighter results in more energy-efficient elevators that are easier to build but harder to design for ride quality. These elevators use raw materials more efficiently but are more vulnerable to various vibrations excited by different components of the system. For example, reducing the mass of the elevator car results in a system that is more sensitive to dynamic excitations generated by the motor, rotating or guiding parts of the car. If not properly considered in the design phase, these factors may lead to poor ride quality. Good ride quality has become a competitive advantage for those elevator companies that can master it because it indicates good design, manufacturing and installation quality (PMT 2018). That is why it is important to understand the dynamic behaviour and response of the elevator car against the excitations generated by different elements of the elevator system. Various methods and tools can analyse the dynamic behaviour of the elevator system or its response to dynamic loadings. The motivation of this thesis is to find the state-of-the-art tools and methods for improving the ride quality inside the elevator car by examining the dynamic properties of the elevator car, namely its nominal modes and frequencies.

1.1 Elevator Systems

Elevator systems can be discretized into several main components depending on the simulation task and the accuracy of the required results. The elevator market divides traction elevators into two main categories: MR (Machine Room) and MRL (Machine room-less elevators). MR elevators have a machine room which includes the machinery and the electrical control units inside the machine room. The MRL-type elevators have all main components installed inside the shaft, leaving the extra space available for other uses in a building. MR elevators have some sub-categories depending on the machine room location for the elevator shaft. In this thesis, the studied elevator system belongs in the MRL elevator

category. Figure 1 represents an MRL elevator with some of its main components. (KONE 2021).

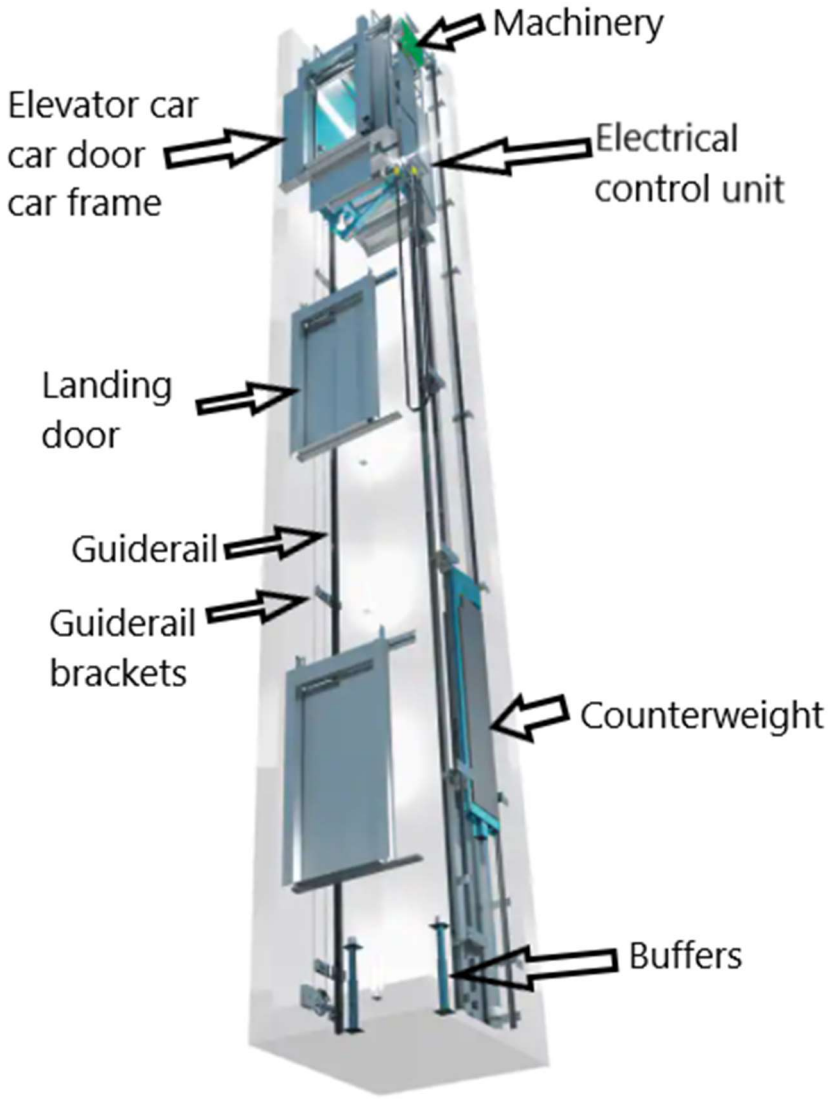

Figure 1. KONE MRL Elevator (KONE 2021).

The complete elevator system includes the components shown in Figure 1: counterweight, machinery and other shaft components such as buffers, guide rails and brackets. Because the elevator type considered in this thesis is electrically driven, the whole system also includes electrical motion control, commonly known as electrical drive.

1.1.1 Elevator Cars

The system that is under investigation is the elevator car. More specifically an integrated car. There are also isolated cars for more high end solutions. The elevator car's function is to carry passengers vertically inside the building safely and comfortably. The elevator car structure can be discretized into three main mechanical components: The elevator car, car frame and the car doors as shown in the figure 2 below. The elevator car is fixed to a frame and typically supported to the upper and lower beams of the frame. The car frame includes the pulleys that suspend the system inside the shaft like the typical MRL configuration is 2:1 roping for passenger elevators. Horizontally, the car system is supported by a set of guide shoes that are fixed to the car frame.

A line of guide rails supports the elevator car via guide shoes when the elevator car moves vertically inside the shaft. The guide shoes support the car from the low- and the top end of the frame. There are two main types of guide shoes, roller guide, and sliding guide shoes. Sliding guide shoes are usually made of some wear-resistant polymer and typically require lubrication of the guide rails. Typical roller guide shoes are sets of wheel with rubber type coating on an aluminum wheel pushed by an adjustable spring towards the guiderail tip.

Figure 2 represents the elevator car system with its main mechanical components. The actual car door assembly is missing from the figure, but its intended location is shown.

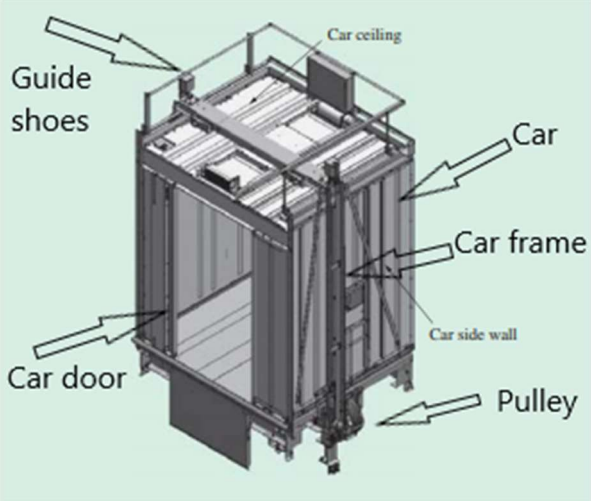

Figure 2. Elevator car system. (Hitachi 2017).

1.1.2 Elevator Ride Quality

The elevator ride quality and ride comfort are separate concepts in elevator industry but they do not exclude each other. The elevator ride comfort is a concept that describes the overall passenger elevator ride experience, including the elevator's aesthetic appearance. Ride comfort can be very subjective. It depends on the expectations of elevator passengers, and factors like their ages and cultural backgrounds. Some individuals may consider the elevator ride comfort to be good when the elevator does not make any noise during its operation and movements are almost insensible. At the same time, other riders expect or are more used to noise and sensing the elevator movements. (Howkins 2007.)

The elevator ride quality covers noises and movements caused by the elevator run. The movements that human passenger’s sense during the elevator run are accelerations and jerks caused by elevator acceleration to nominal speed and other structural excitations such as elevator running past guide rail joints. The human body's response to the horizontal and vertical vibrations affects the passenger's experience during the elevator ride. Humans can sense the horizontal accelerations occurring at lower frequencies. Higher horizontal frequencies do not excite whole-body vibrations horizontally. The frequency range for harmful human-body vibration is from 0-100 Hz. The passengers are also subjected to

vertical vibrations which are higher frequency vibrations caused by machinery or pulley rotations. Elevator car structure usually absorb these frequencies, but sometimes, the vibrations cause poor ride comfort experiences because of poor design. (Howkins 2007.)

The ride quality for an installed elevator is assessed by measuring the in-car vibrations and noises produced during the elevator run. The instruments used to measure the vibrations can be used to analyze the frequencies that excite human organs. For example, the resonant frequencies for the human head vary from 20-30 Hz and for the eyeball from 20-90 Hz. Most of the different resonant parts of the human body are from 0-90 Hz. If exposed for a long time, these frequencies affect the passenger's comfort and potential health. The impact on the ride comfort caused by vibrations varies from person to person. Humans also sense higher frequencies, but they cause mostly mild discomfort. (Szydlo et al. 2019.)

1. 2 Objectives

This thesis aims to perform a successful dynamic analysis for elevator car systems. The dynamic analysis results should be examined to improve the elevator car system ride quality. The ride quality can be improved by reducing the in-car vibration amplitudes occurring during the elevator run. In practice, this process is done by performing dynamic analysis with software utilizing the meshless method. The modal and the harmonic response analysis are the dynamic analysis types used. The harmonic analysis is used to understand at which frequencies the car floor centre is most sensitive. The mode shapes from the modal analysis are studied to point out how the design of the elevator car system must be adjusted to improve the ride quality.

1.2.2 Research questions

The research questions for this thesis can be set out followingly

1) Can the meshless method be utilized in the dynamic analysis of elevator car systems more effectively than more traditionally used element methods?

2) What are the nominal frequencies and modes that are the most relevant for elevator ride comfort?

3) How can we utilize the new faster meshless analysis methods to design an elevator car with better performance in ride quality?

1.2.3 Methods and Framework

The analysis software used in this thesis work is SimSolid which utilizes a meshless method, thus, providing an opportunity to perform analyses on large assemblies faster than more commonly used FEA software that requires meshing. The SimSolid software can perform similar analysis that other typically used FEA software, including static, thermal, and dynamic analysis. In this thesis, the focus is on modal and harmonic response analyses. (Altair 2021.)

A dynamic analysis performed by finite element analysis was applied to the case studies. The case studies for this thesis were performed from the machine dynamics framework. The dynamic analysis results are then examined on their impact on the ride quality of the elevator car. The meshless element method was used in the analyses. The hypothesis to test is if the dynamic analysis performed by meshless method can be applied to ride quality assessment of the elevator car system.

1.3 Validation

The results will be validated by measuring the movements inside the car during the elevator run on the actual prototype unit. The measurements for ride quality provide quantitative results on the elevator performance. In practice, the results are accelerations in lateral and horizontal directions and the sound produced during elevator operation. During the run, the amplitudes are measured in the time domain. The results in the time domain can be transferred to a frequency domain, for example, through Fast Fourier Transform (FFT) to analyse the root causes of the ride quality results (PMT 2018).

1.3.1 Qualitative and Quantitative Ride Quality Assessment

Defining the elevator ride quality is based on two main standards. ISO 18738 standard sets definitions for the ride quality measurements and ISO 8041 defines the specifications for the vibration measurement in terms of human response to the vibrations. Standardization does not set strict limits on what is acceptable ride quality. Instead, the standards set out how the ride quality should be measured. Setting clear standard limits on the ride quality is not very productive as what might be considered good ride quality today may not be accepted in future. However, the elevator manufactures have set certain boundaries on their products. (PMT 2018.)

In the past, before proper analog instrumentation the ride quality assessment of the elevator was purely based on the "feel" of the elevator ride experience. This subjective measurement led to certain obvious problems. For example, the outcome of such assessment could have been affected by the mood of the person performing it. Also, the assessment relied on individual's memory on how the good ride quality should sound and feel like to which humans were not clearly calibrated. (PMT 2018.)

Qualitative ride quality measurement became possible in 1960 when analog instruments for measuring mechanical movements were available. The sound measurement devices were available for some time. However, instruments that were able to measure the physical movement of an elevator car during the elevator run made the measurement of elevator ride quality possible. The commonly accepted quantities, vibrations, acceleration jerk and sound level were chosen to define the ride quality of an elevator. The first velocity sensors used were simple but did not provide much efficiency in measurements. The accelerometers could provide information in multiple directions at a large range of frequencies. Furtherly, the developments of digital instruments offered easier use, which then became tools that are used in the industry. The signal recorded during the elevator run is examined by evaluating the peak values of the signal. In case of accelerations, the results are usually shown in the units of Gal (Galileo) that is 0.01 $\mathrm{m/s^2}$. (PMT 2018.)

Vertical transportation usually causes noises and vibrations, which are then perceived as the ride quality of the elevator by the elevator passengers. The physical movements affecting the ride quality of an elevator car can be caused by many different parameters such as elevator control logic, installation quality and the construction of the elevator car itself. The excitations may come from guide rail joints, roller guides or machinery rotation. Also, the elevator velocity and acceleration control affect the ride quality experienced by elevator passengers. (Li et al. 2004, p. 69-70.)

1.3.2 Ride Quality Measurement and Analysis

The measured quantities like in-car accelerations should be introduced in maximum peak to peak values and in A95, value which stands for the maximum value less than 95% of peak values. The processing of measured data is further defined in the ISO 8041, a standard for measuring instrumentation. (ISO 18738 2012, p. 4-5.)

The challenge for creating software and instruments arises from considering the dynamic behaviour of passengers inside the elevator car. Passengers human body can be considered as the component inside the car, which interface to the car floor must be considered. The ISO 8041 standard sets guidelines for the instrumentations for considering human feet pressure acting on the car floor. (Herrera & Kaczmarczyk 2009.)

The common instrument for measuring the ride quality is the Elevator Vibration Analysis instrument (EVA) which is also used to validate of the case studies in this thesis. EVA can be used to measure elevator physical movements during elevator run according to the ISO 18738. During the elevator run, which is meant to be from the lowest floor to the topmost, quantities such as sound and physical movement including speed, position, jerk and acceleration are measured. The outcome of the measurements results is in Figure 3. There are four graphs in the figure above in the time domain corresponding with the whole time of the measurements. The top graph is the sound level during the measured time and the graphs

below are the accelerations on all axis. In the EVA measurements, the Z-axis stands for vertical and Y & X for the lateral directions. Also, close to the graphs above the plots are maximum peak-to-peak (Pk/Pk) values, A95 value and zero to-peak (0-pk). (PMT 2018.)

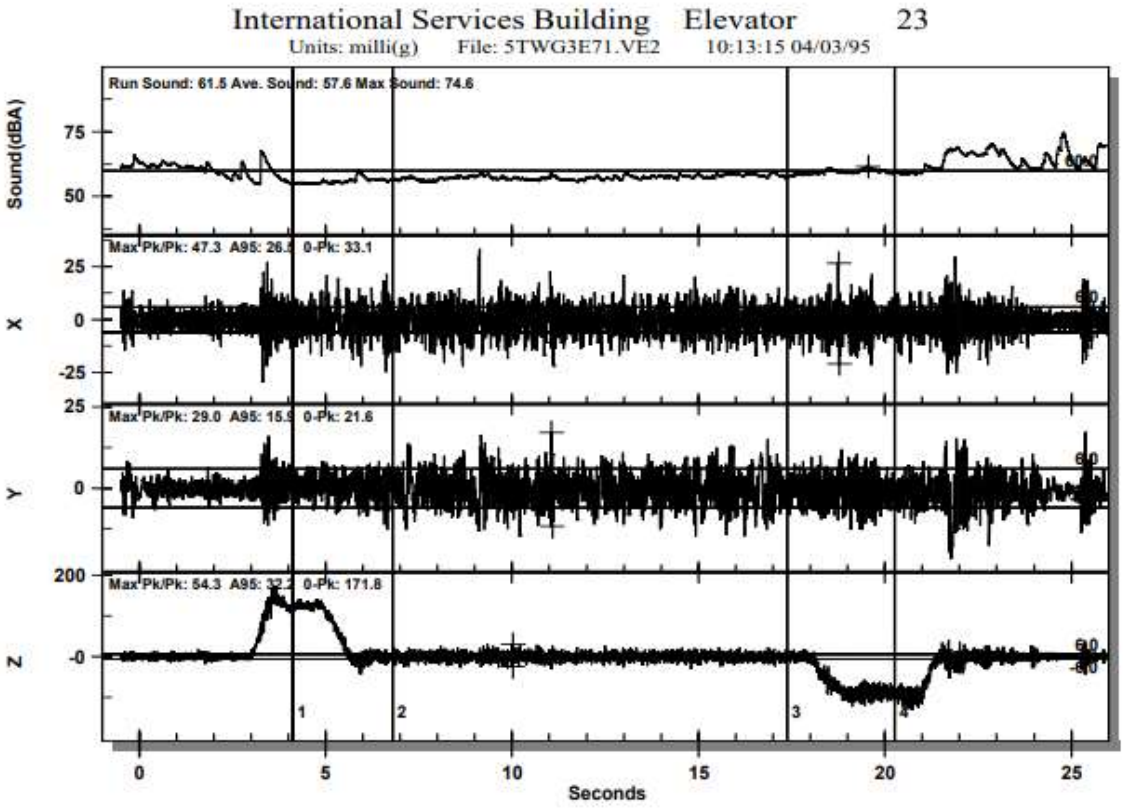

Figure 3. EVA measurements results. (PMT 2018.)

The whole measurement history itself does not give the ride quality analysis information. That is why the data from the measurements are divided into different regions, acceleration, full-speed and retardation, especially because the vibrations should be evaluated at full-speed (PMT 2018). The regions are split by the boundaries defined by the ISO 18738 standard. The boundaries are set to the beginning of the acceleration after door closing and the beginning of the full speed at more than 0.5 m above the first landing. After full speed is the initiation of elevator speed retardation and arriving on the last floor after door opening.

In some cases the door opening and closing can be excluded from the full speed if the door operation is causing high amplitude in car movement by agreement. (ISO 18738 2012, p. 5.)

In order to analyse the root causes for the elevator ride quality performance, the response in physical movement is transformed from the time domain into the frequency domain. This is done by an FFT (Fast Fourier Transform) method. FFT is a modification of the Discrete Fourier Transform. The FFT is an quicker alternative to the Discrete Fourier Transform as it requires less complex multiplications. The FFT is commonly used and is available as code in almost all computation platforms such as Matlab. (Braun, Ewins, Rao 2002, p. 1342-1343). The FFT can be understood as a fingerprint of the elevator car's excitation frequencies during the elevator run in the ride quality analysis. For example, once the measurement indicates a poor ride quality with the help of the FFT, it is possible to point out at which frequency the highest amplitude is occurring. Knowing the elevator systems parameters like the diameter of roller guide or car frame pulley can help define at which frequency that particular component excites the system. Analysing the resonance of flexible components requires a numerical analysis like meshless methods utilized in this thesis. The excitation frequency of the rotating component can be defined by the following formula that is based on the constant angular velocity (Mäkelä et al. 2012, p.93.)

$$f_o = \frac{v_e}{\pi D_d} \tag{1.1}$$

Where the v_e term stands for the elevator nominal or measured speed and the D_d the diameter of a rotating component. If the peak amplitudes indicate any rotation part or electrical excitation, the dynamic analysis should be carried out for the elevator car system. Like in this thesis, the ride quality of an elevator car is assessed quantitatively using the dynamic analysis.

2. Theory of Finite Element and Dynamic Analysis

This chapter introduces the background theory of the methods used in the case studies. The SimSolid software used in the case studies utilizes the meshless the method. In this chapter, the traditional finite element method is compared to meshless methods. In order to have an introduction on the differences between what is traditionally considered as the finite element method and the meshless method the background of both methods is introduced.

The case studies were based on the dynamic modal and harmonic response analysis. The theory regarding the finite element method concerns the static analysis case, but similar approaches and principles are utilized in the dynamic case. The main subject in the finite element methods is the assembly of the stiffness matrix associated with the sub-structure which in practice is a single element or part inside structure assembly. A mass matrix for the sub-structure is also formed in the dynamic case. Forming a mass matrix may require similar approaches like forming the stiffness matrix.

2.1 Finite Element Method

The traditional FEM is powerful tool for analyzing structures with complex shapes using simple shaped elements in the structural analysis field. From the mathematical approach, the finite element method is a way to obtain approximate solutions to problems that cannot be solved by a closed-form solution (Mac Donald 2011, p.2-4.)

The FEM is mostly known for its applicability in stress analysis of structures, but it is also widely used in dynamics and thermal analysis. There are many other applications, such as fluid dynamics, where the analysis also utilizes FEM techniques like in a as computational fluid dynamics. In these chapters, FEM is discussed from the structural analysis and dynamics approach.

Typical FEM procedure includes the discretization of the problem, which in practice is a structure. A structure having complex geometries is split into finite elements. These finite elements are connected to each other via points called nodes forming a mesh. The meshing of the structure is part of the analysis task discretization and can be done manually or by FEM software built-in features. Sometimes the meshing itself may require some sub-tasks depending on the structure under investigation. Some local features like holes may require a finer mesh to be defined properly, so the structure may have to be divided into sub-structures. A Figure 4 represents a typical process of structural analysis done by FEM. In Figure 4 the size of the larger sizes of arrows on discretization and post-processing indicate that these steps are most involved for the user of the finite element analysis (FEA) software

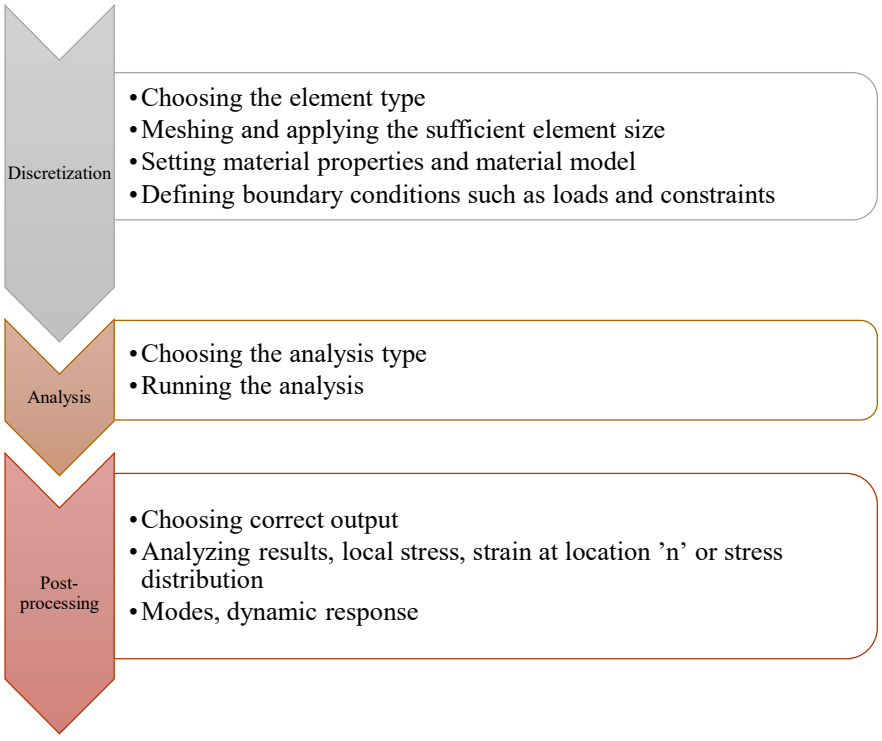

Figure 4. Simplified general level FEA process while using software utilizing FEM.

Depending on the complexity of the structure or system, the actual time-consuming step might be the analysis. However, this depends on the software and hardware performance and actual computational effort required due to the complexity of the analysis. However, the analysis part is not so involving for the end-user.

It can be said that state-of-the-art FEA usage can discretize the structure to a sufficient size, meaning choosing the correct element size or type and utilizing the symmetry of structure if possible. After the analysis is done, it is important to be able to describe how the results relate to the real-world problem.

Nodes are points that connect the elements forming a mesh and are used to describe structural behavior mathematically. For example, in the case of structural analysis, each node is associated with a local field variable such as displacement so typically in structural analysis FEM calculates displacements at each node. These field variables can be other quantities depending on the analysis type carried out, but typically they are temperature or displacement. An element matrix predicts the nodal changes in the field variables inside the elements. In the case of structural engineering, that matrix describes the displacement resistance and is called the stiffness matrix. The forming of the stiffness matrix requires a matrix of shape functions and a strain displacement matrix that are used to approximate the displacements between the nodal points inside the elements. (Pavlou 2015, p. 2-5.)

2.1.1 Shape Functions

Shape functions are used to interpolate the nodal changes of field variables within the element. They are typically a polynomial function whose polynomial degree depends on but is not limited to the element type. Typically, more complex elements with more degrees of freedom are described with higher degree polynomials. The elements formed with higher degree shape functions can provide more accurate approximations for the exact solution. However, the computational accuracy can also be altered by adjusting the location of the nodes or increasing the number of elements. (Rao 2018, p. 84.)

Suppose the analysis problem can be solved in a single spatial coordinate like bar under axial loading, which is deforming in one direction. In that case, we can use a one-dimensional line element that can be interpolated with a linear model. The interpolation function for the linear

model is a first-degree polynomial. The higher order elements have additional nodes added mid-element between corner nodes. Higher order elements require higher order interpolation for their shape functions. The usage of the higher-order elements is justified in FEA when the change of the field variable is very rapid at the local locations of the structure, such as stress peaks. (Rao 2018, p. 82-84.)

If we consider a one-dimensional line element but now as a beam with two degrees of freedom on each end, rotational and translational, we need to describe it as a third-degree polynomial to interpolate with all in total four degrees of freedom. So, the degree of polynomial shape function must correspond to the degrees of freedom that the element used to form with this shape function has. (Rao 2018, p. 344.)

The one-dimensional bar element can be described with a linear interpolation model with one field variable for axial displacement. The following interpolation model *u(x)* is suitable for such elements. (Rao 2018, p. 83.)

$$u(X) = c_1 + c_2 X \tag{2.1}$$

Where,

X	single field variable
c_1	first interpolation unknown constant
c_2	second interpolation unknown constant

There are many ways to use the interpolation model to form a set of shape functions. In terms of nodal values, we use global positions of element nodes. Another approach is to use local coordinates of an element or natural coordinates. The Figure 5 illustrates the interpolation model. (Mac Donald 2011, p.83-87.)

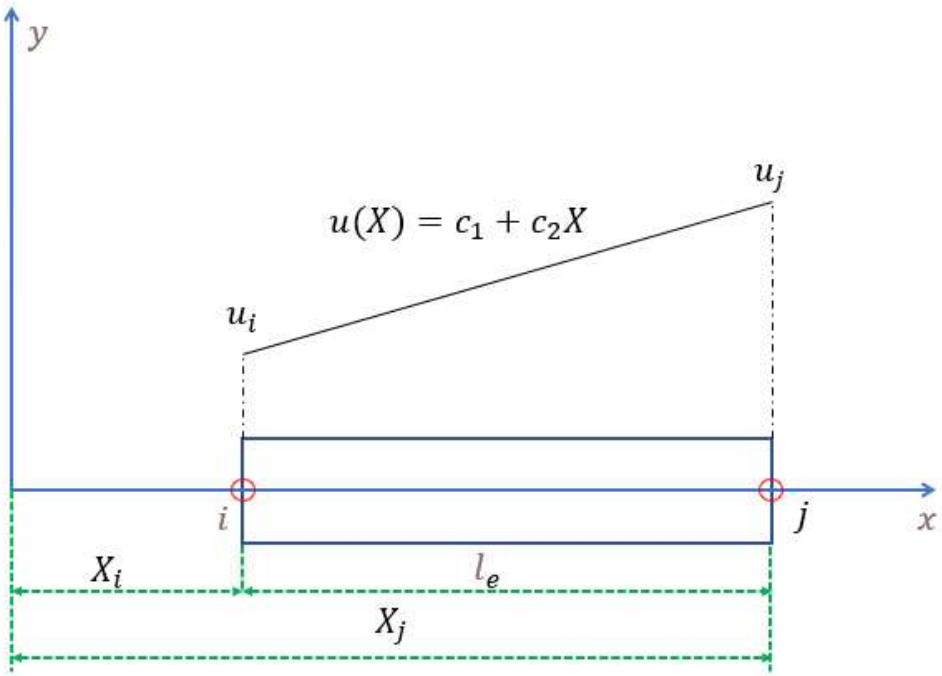

Figure 5. Linear interpolation model of the 1-D element.

For each nodal displacement u_i and u_j, we get equation based on the interpolation model on Equation 2.1 (Mac Donald 2011, P.83-87).

$$u_i = c_1 + c_2X_i \tag{2.2}$$

$$u_j = c_1 + c_2X_j \tag{2.3}$$

Solving the constants, we get two shape function S_i and S_j.

$$S_i = \frac{X_j - X}{l_e} \tag{2.4}$$

$$S_j = \frac{X - X_i}{l_e} \tag{2.5}$$

Where,

l_e element length

Now if the shape functions were to be set as in terms of local coordinates so that the coordinate system is aligned at the element first node (on the left, Figure 5). The shape functions S_i and S_j would be following (Mac Donald 2011, p.83-87).

$$S_i = 1 - \frac{X}{l_e} \tag{2.6}$$

$$S_j = \frac{X}{l_e} \tag{2.7}$$

In the case of beams the interpolation, the model should be able to approximate translation and rotation at each node. The higher degree of polynomial required is a cubic model with four interpolation variables, like on the Equation 2.8 (Rao 2018, p.83).

$$u(X) = c_1 + c_2X + c_3X^2 + c_4X^3 \tag{2.8}$$

2.1.2 Element types

In order to discretize the analysis task into a sufficient model, a correct element type must be selected. Type of results and the structure under investigation are some of the main factors when choosing the element type. The simplest elements used in FEM are one-dimensional spring elements. Spring elements behavior can be described by Hook's law, where the displacement, depends linearly on the applied force.

$$F = k(x_2 - x_1) \tag{2.9}$$

The stiffness of these elements is defined by a stiffness coefficient k. The term $(x_2 - x_1)$ refers to the elongation of the springs. The relation between the force and displacement or elongation is linear in Equation 2.9. Some special spring elements model the relation between force and displacement non-linearly. Hence, the model used in 2.9 is usually referred to as the model of linear spring elements. The stiffness coefficient k describes stiffness of a single spring element. The global stiffness matrix of spring elements is formed by knowing the stiffness of each element and how the elements are connected. (Pavlou 2015, p. 44.)

The 1D bar elements are similar to spring elements as they describe the only displacements in axial direction. This element is similar to Figure 5, where the linear interpolation model is described. The displacements that the 1D bar elements can describe are caused by compressive or tension loads. Computation of exact solution for the bar under axial loading is not a complicated problem and can be solved using the strength of materials formulas. If the structure is a bar consisting of two or more pieces having different cross-sections or material properties, the problem of axial translation becomes more complicated, and the use of FEM can be justified. (Mac Donald 2011, p.90-91.)

When doing a FEM computation for beam structures, an element called beam element is available. Definition of a beam is typically a long slender structural part that carries the load by bending moment. A typical application of beam elements is constructions, crane girders and bridges (Mac Donald 2011 p.108-110). Simple beam problems can be solved by utilizing statics and strength of material formulas without the need for the FEM approach. However, in large structures or the case of hyperstatic beams, a FEM usage might be justified. Also, dividing the beam into finite elements allows the determination of the displacement at a certain location. In the case of the dynamics, we can discretize the beam into finite elements so that the nodes represent the points of interest or we are interest in certain number of flexible modes. Figure 6 shows the beam element mesh with rendered cross-section.

Figure 6. Beam element mesh with cross-section (Kurowski 2016, p. 26).

As the beams are expected to carry loads by bending, in FEM modeling their elements should include rotational displacements and translational displacements at the nodes located at both ends of the element. The interpolation model that can approximate the displacements and rotations at the end of the beam elements is introduced in Equation 2.8. Figure 7 represents the displacements of the beam element.

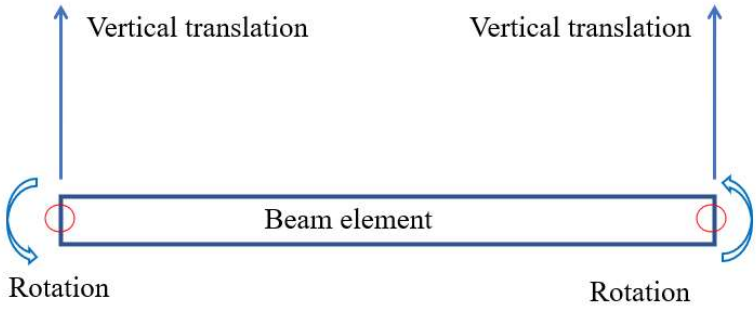

Figure 7. Displacements of the beam element.

Having more than just a one-dimensional representation of the structure leads to having a 2D elements. The simplest 2D elements are the plane stress or plane strain elements. The plane stress elements can compute stresses only in plane of the element. The plane stress elements can compute strains out-of-plane. The plane strain elements on the opposite can compute the strains in-plane and stress out-of-plane (Debney 2020, p.48). These elements have their material properties included differently in the stiffness matrix. The plane stress

analysis performed by the plane stress elements is suitable for structures consisting of thin sheets that are under tensions. The plain strain elements are suitable for analysis of structures such as long beams with constant loading, dams and pressure vessels. (Mac Donald 2011, p.118-119).

A more complicated type of 2D element type is a plate element. Plate elements, are suitable for analyzing membranes and continuous beams which thickness does not vary. These elements are used in applications where bending of the plate is not considered. The shell elements are the type of elements that take both, membrane and bending into account. The ability to describe the curved structures with the plate elements and the fact that the bending and membrane forces can be taken into account make the element properties of shell difficult to define. Figure 8 represents meshes constructed with 2D elements. (Mac Donald 2011, p.142-145).

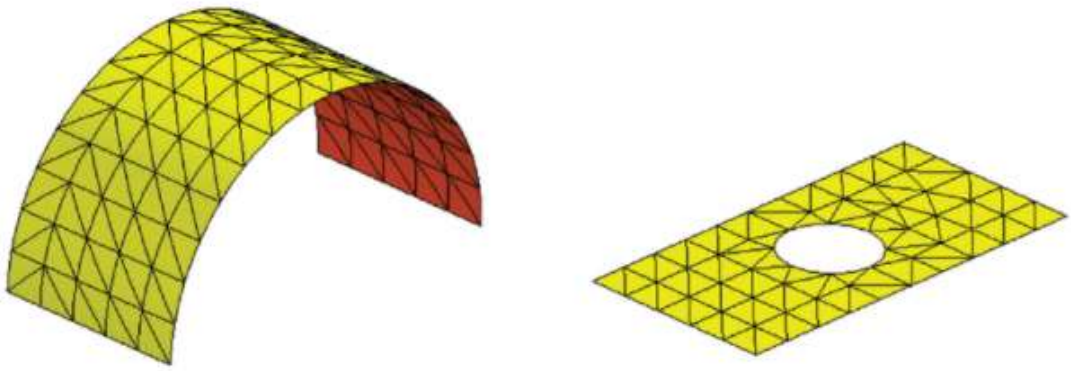

Figure 8. 2D elements, membrane element left plane or plate element right (Kurowski 2017, p. 24).

As in reality, almost all real-world structural problems are three-dimensional, so simplified 1D and 2D models are not always sufficient. When a whole 3D representation of the analysis problem must be utilized a 3D elements are available. The 3D elements, also known as volume elements are sufficient to be used when the structure under investigation is more complex in geometry. One of the advantages of using 3D elements is that the structure model can be on the FEA software as it would be in real life. Figure 9 represents a mesh generated

from solid elements with a full representation 3D of the structure. (Mac Donald 2011, p. 146-148).

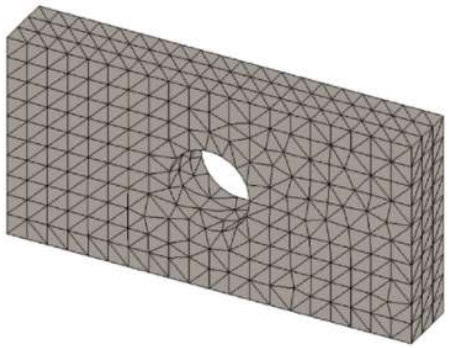

Figure 9. Mesh with solid elements (Kurowski, 2017, p. 24).

3D volume elements are the most complicated elements. Usually meshes that are done by 3D elements require more computational speed. Also, the postprocessing of the analysis results becomes more complicated with 3D elements. (Mac Donald 2011, p. 146-148.)

The 1D, 2D, and 3D elements have different interpolation models because when the single element has higher degrees of freedom between, the interpolation model must be of higher order. Higher-order interpolation with the help of a higher number of interpolation coefficients can be used approximate a higher number of translations or rotations. Element stiffness matrix describes the element properties like displacement resistance. In case of bar elements the stiffness matrix is used to solve the translations at the nodes. With the beam elements the rotations are solved in addition to translations.

Forming the stiffness matrix requires the material and cross-sectional properties to be known and the shape functions. The shape functions are used to form a strain displacement matrix for the element (Mac Donald 2011 p.111). In the case of bar elements, the strain displacement matrix can be formed followingly (Mac Donald 2011, p.90-91).

$$\mathbf{B} = \begin{bmatrix} \frac{\partial S_i}{\partial X} & \frac{\partial S_j}{\partial X} \end{bmatrix} \tag{2.9}$$

In the case of the beam elements, the strain displacement matrix would require application of the beam theory. When applying the energy method the stiffness matrix for the bar element is formed as following.

$$\mathbf{K}_b = \frac{EAl_e}{2} \int_{-1}^{1} [\mathbf{B}^T \, \mathbf{B}] dx \tag{2.10}$$

Where,

$\mathbf{K}_b$	Stiffness matrix of the bar element
A	Cross-section the area of element
E	Young's modulus

For the beam element the principle is similar. As the beam element is able to describe also rotations the cross-sectional property is moment of inertia instead of area. The stiffness matrix describing the beam element stiffness properties can be defined followingly.

$$\mathbf{K}_{be} = \int_0^L \mathbf{B}^T \mathbf{B} \, dx EI \tag{2.15}$$

In both, beam and bar elements, an interpolation model that approximates the translations between the nodes must be set to compute the stiffness matrix of the element. In both cases, the strain displacement matrix is computed, which used for the stiffness matrix. For the 2D and 3D elements the stiffness matrix computation becomes more complex but utilizing the interpolation model remains.

2.1.3 Boundary Conditions

Setting the boundary conditions, means in FEM, applying loads and constrains. The constrains of nodes or elements are like assembly fixings of the structure. Like in real-life assemblies or structures using welding or mechanical connections, we can fix the parts rigidly to each other to restrain some of the displacements or rotations. Also, the soft springs that limit or cancel rigid body motions can be understood as constraints. Whether the fixing on the assembly provides similar restrictions as on the FEM model is up to the judgement of the FEA software user. (Kurowski, 2004, p. 64.)

Basically, all loads except volume and body or inertia-loads are boundary conditions. The loads are typically easier to set than constraints and usually cause fewer computational errors. The magnitude of the FEA results usually can indicate if the loads are set correctly on the FEM model. (Kurowski 2004, p. 64-65.)

While applying fixed constrains to a structure at a particular location, the assumption is that there are no translations or rotations allowed in that particular point or node. These assumptions must reflect the actual structure. Setting wrong boundary conditions can lead to inaccurate FEM computations making the analysis effort obsolete. The boundary conditions should not allow any translations and rotations where they do not occur on real-life systems and allow them where these deformations actually occur. (Mac Donald 2011, p. 229-231.)

2.2 Meshless Methods

As stated in the previous chapters, the traditional way of FEM is a structure discretization into smaller finite elements that form a mesh. The popularity of this approach is because of its flexibility for even complex structures. However, the traditional mesh-based FEM is not flexible enough to utilize different numerical methods due to its strict nature of having nodes in a predefined manner. The FEM is also vulnerable to numerical errors in some cases, such as large deformations. These issues caused by the strict nature of FEM meshing resulted in

evolution of meshless or meshfree methods (Liu & Gu 2005, p. 37-39). The FEM is an approximate method, and the accuracy depends on the discretization of the problem. This approach gives the user of the FEA software responsibility for how well the results describe the actual physical system behavior. The discretization, including detailed meshing and simplification of the FEA model can be so labor-intensive for the analyst that in can impact the total design or development project cost (Liu & Gu 2005, p. 37).

Many of the problems in engineering science can be solved by simple algebraic equations, however, due to the complex nature of most of the practical problems, approximative numerical methods have been developed. The most popular numerical approximation methods are the finite difference method, FEM, boundary element and meshless method. (Liu & Gu 2005, p. 44-46.)

The motivation for developing the meshless method came from simulating demanding manufacturing processes dealing with very large deformations. Initially, the problem with the mesh-based approaches for such simulations raised from the mesh structure and limited possibilities of treating discontinuities that do not coincide with the original mesh lines. Compared to FEM, the objective of meshless solutions is to remove the need for structure discretization by smaller elements and instead describe the structure only by a set of nodes or points used for approximation functions. (Belytschko et al. 1996.)

The FEM approach can also be applied using the variational approach and the weighted residual approach. The variational approach is based on the variational calculus that deals with the extremization of the functions in terms of integrals (Rao 2018, p. 174-175). The variational approach can be applied using the of minimum potential energy approach to minimize the integral function. Solving the minimum potential energy problem by the variational calculus can become handy with structural problems such as bar under axial loading with variable cross-section, so that cross-section A can variate as $A=A(x)$ (Pavlou P. 2015, p. 34-35). In the traditional FEM computation, this example would mean that the generated mesh should be so dense that it describes the varying cross-sections sufficiently. The weighted residual approach means that the element matrices are derived directly from

the governing differential equations (Rao 2018, p. 174). The variational Raleigh-Ritz methods and weighted residual-based Galerking methods can be found from literature commonly while studying FEM or meshless methods, but for the method to be called meshless method it requires further development.

The meshless methods are similar to FEM, but the main difference is that instead of mesh generation, a set of nodes is generated inside the structure's domain. Also, instead of having strict pre-defined element-based shape functions, the meshless method has shape functions based on nodes in a local support domain. Table 1 summarizes most of the differences between the meshless or meshfree (MFree) element method and FEM. (Liu & Gu 2005, p. 44-46.)

Table 1. Differences between FEM and meshless/meshfree methods (Liu & Gu 2005, p.41).

Items	FEM	MFree method
Mesh	Yes	No
Shape function creation	Based on pre-defined elements	Based on local support domains
Discretized system stiffness matrix	Banded, symmetric	Banded, may or may not be symmetric depending on the method used.
Imposition of essential boundary condition	Easy and standard	Special treatments may be required, depending on the method used
Computation speed	Fast	Slower compared to the FEM depending on the method used.
Accuracy	Accurate compared to FDM	More accurate than FEM
adaptive analysis	Difficult for 3D cases	Easier
Stage of development	Well developed	Infant, with many challenging problems
Commercial software packages availability	Many	Few

As table 1 mentioned, the meshless might be slower in computational speed, but it can provide results more quickly because meshing is not required. However, careful discretization of the structure allows the analyst to read the results of field variables like stresses or displacements from the desired location. Computational accuracy is an issue that depends on the actual system or structure under consideration. In traditional FEM, the computational speed can be adjusted by choosing various element types or the number of nodes by refining the mesh. Choosing the element type also allows understanding how well the analysis results translate to the actual real-world structure. The drawback of element selection and discretization is that selecting the correct element type and size requires an experienced user. Sometimes, the analysis must be performed in multiple iterations to find suitable element type and size.

Currently, many fall under element free or meshless method category. They can be classified in terms of formulation procedures and function approximation schemes. The formulation procedures are roughly split into weak and strong form methods. The strong form of approximation is done by solving the exact governing partial differential equations, thus requiring consistency for the unknowns of the unknown solved function. The weak form requires a weaker consistency on the approximate functions, and it is more applicable in the higher complexity problems (Liu & Gu 2005, p.45). For example, the Weighted residual method or Galerkin method which are used meshless methods belongs to group of weak form methods (Rao 2018 p. 174).

2.2.1 Procedure of Meshless Methods

The first step of the meshless element method is the domain representation of the structure. A scatter of points is located in arbitrary locations in the domain and its boundaries. However, the location of these points is not always arbitrary over the whole elements but can be altered by different techniques in the meshless method implementations. These techniques usually split elements or parts into sub domains. Inside these sub-domains, algorithms that recognize geometrical features can guide the point density in locations of interest. Some solvers can increase the point density during the iteration runs at the locations

where the high field variable gradient is expected. Figure 7 represents adaptive point refinement for a plate with a crack problem analyzed by meshless methods. (Liu 2010, p. 700-705).

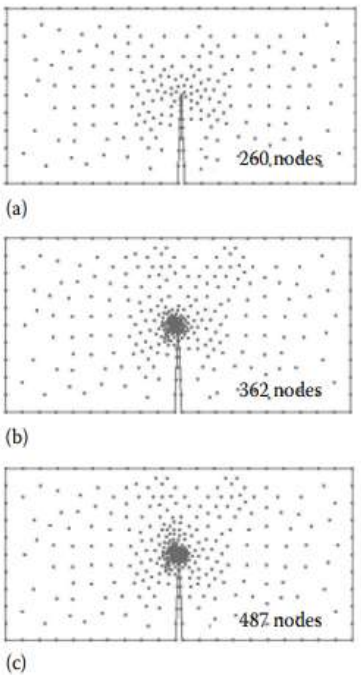

Figure 6. Plate with a crack problem analyzed with meshless method (a, b and c are the same plate with different point scatter) (Liu 2010, p. 702).

These points represent nodes that represent field variables and are sometimes referred to field nodes. The density of these nodes depends on the required accuracy and how the code processes the structure. However, some of the meshless method codes can adapt the solution with higher node density to increase the accuracy locally even so that the initial node distribution is not important (Liu & Gu 2005, p.41-42). The traditional FEM has a different approach with node placement and domain of the structure representation. As mentioned in earlier chapters, the principle of the traditional FEM lays on the strict elementwise discretization and connection of the elements via nodes. Figure 6 represents the differences between the meshless domain-based approach and the traditional FEM approach.

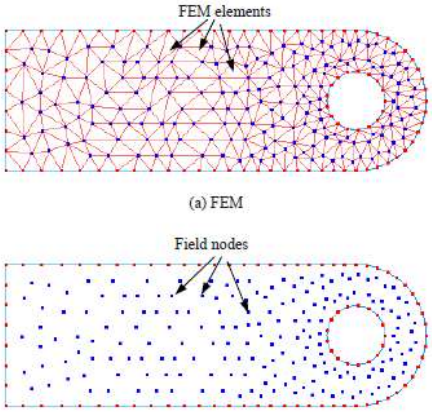

Figure 6. Finite element mesh (upper) and a meshfree structure domain. (Liu & Gu 2005, p.42)

The next step is the function interpolation or approximation. The interpolation and approximation in meshless methods are done within a smaller subdomain inside the main domain of the structure. The subdomains are usually referred to as support domains. As in the traditional FEM, these nodes represent a field variable such as displacements. The function of the field variables can be formulated followingly (Liu & Gu 2005, p.43).

$$u(x) = \sum_{i=1}^{n} \phi_i(x) u_i = \mathbf{\Phi}^T(x)\mathbf{U_s} \tag{2.16}$$

Where,

n	number of nodes at local support domain of the point x
u_i	the local field variable of i node
$\phi_i(x)$	shape function of the i node
$\mathbf{U_s}$	Vector of field variables
$\mathbf{\Phi}^T$	Vector of shape functions

As mentioned in chapter 2.1.1, the traditional FEM utilizes the shape functions to formulate the element matrices to describe structures behavior in different types of problems. The shape functions have a more flexible nature inside the domain boundaries in the meshless methods.

The forming of the system equations in the meshless methods is done by shape functions and by strong or weak form system equations. These equations are used in nodal matrix form and then are assembled in a larger global system matrix. The nodal matrix is similar to element matrix used in the FEM approach. Solving the global matrix is done similarly to traditional FEM. As the inverse of the matrix is a computationally heavy procedure, the solvers utilize methods such as Gauss eliminations, LU decomposition or some iterative means. Also, the eigenvalue problems have multiple different solvers. (Liu 2010, p. 21-22.)

2.2.2 Shape Functions in Meshless Methods

There are many different approximations and interpolation techniques for the meshless methods. Based on the literature available, the moving least square method is the most popular technique for meshless interpolation. Like in the traditional FEM, these interpolation techniques are used to create shape functions. In order to create a function approximation in meshless methods, it is necessary to specify the form of the functions to be used in approximation (interpolation model) and define the approximation procedure.

The basis of the good shape function is that it can deal with scattered arbitrary nodal distribution inside the element domain or sub-domain. The shape function forming technique should be numerically stable enough to describe the physical problem. The numerical stability issue arises when the node density is particularly large and irregular. Additionally, the shape function interpolation technique should provide computational efficiency. (Liu & Gu 2005, p.43.)

The least square is one of the methods that is used to form approximation shape functions in meshless methods. The idea of the least square method minimizes the square distance between data values defined at the certain points used to evaluate the approximating function. If the approximation functions should provide better accuracy at a certain point a weighted least square fit can be utilized. The moving least square method was developed to generate smooth approximate functions for general surface generation problems. The moving least square method is similar to weighted method but instead of choosing arbitrary point to have more weight, in the moving least square method, it is done to each point. (Taylor & Zienkiewicz 2000, p. 431-438.)

The moving least square technique for creating shape functions can be applied as on 2.17 (Liu & Gu 2005, p.55).

$$u^h(x) = \sum_{i=1}^{m} p_i(x) a_j = \mathbf{p}^T(x)\mathbf{a}(x) \tag{2.17}$$

Where,

$p(x)$ basic function of spatial coordinates

m number of basic functions

$\mathbf{a}(x)$ vector of unknowns

The *p(x)* is formed from the Pascals triangle monomials. The vector of unknown coefficients is solved through weighted discrete obtained from the support domain. A complete vector of shape functions is following (Liu & Gu 2005, p. 97-98.)

$$\mathbf{\Phi}^T(x) = \mathbf{p}^T(x)\mathbf{A}^{-1}(x)\mathbf{M}_{mls}(x) \tag{2.18}$$

Where **A** is the weighted moment matrix created using the arbitrarily distributed weight functions of node coordinates *W(x-xi)*. And the $\mathbf{M}_{mls}$ is the 3xn matrix formed of the nodal coordinates inside the domain (Liu & Gu 2005, p. 98).

2.2.3 Element-free Galerkin Method

The element-free Galerkin method (EFG) has shown better convergence and accuracy than traditional FEM and hence has attracted attention in computational mechanics' research. An EFG has been one the most successful among various other researched meshfree methods. The advantage of EFG compared to traditional FEM lies in the usage of smooth shape, functions, which can be enhanced with careful choosing of weight functions for the moving least square interpolation (Belytsckho et al. 2014).

The EFG uses the moving least square method for obtaining the shape functions. Once the shape functions are created, defining the element properties similar to traditional FEM. The element matrices are formed similarly to traditional FEM. The element stiffness matrix requires a strain displacement matrix **B** formed utilizing shape functions and governing elasticity theory. The element stiffness of the domain is formed followingly (Belytscho, et al. 2014).

$$\mathbf{K} = \int_{\boldsymbol{\Omega}} \mathbf{B}^T \mathbf{D} \mathbf{B} d\Omega \qquad (2.19)$$

Where,

D Material and cross-sectional properties, EI

Ω Domain of the element

Comparing the EFG method to the traditional FEM static case, solving the displacements is rather similar. In the EFG case, the force vector becomes more complicated as its sum of

integrals is taken from inside domain and domain boundaries with shape functions and boundary conditions of the elastostatic problem. (Belytscho, et. al. 2014.)

2.2.4 SimSolid Method

The SimSolid utilizes a meshless method, theory of external approximations. In the term of external approximations, the word external refers to set of functions that do not belong to Sobolev spaces at every refinement step. In the case of structural analysis these are functions with finite strain energy. (Altair 2021.)

In the implementation of the meshfree method in the SimSolid, the basic functions of the finite elements are not pre-defined. The functions defining elements are constructed during the solvers run. The solver finds the basic functions of the elements. The element shape functions are not pre-defined. They can be any generic basis functions, unlike with traditional FEM, which element shape functions are strictly predefined. The approximation function of the element is following. (Altair 2021.)

$$U_h = \sum_{i=1}^{n} a_i\,(U)p_i + \sum_{k=1}^{N}(\int_{\Gamma} g_k \gamma U d\Gamma)p_k \tag{2.20}$$

The term $\int_{\Gamma} g_k \gamma U d\Gamma$ stands for the boundary DOF where U is the function to be approximated on the element. a_i are the coefficient of the internal elements and p_i are the internal basis functions of the element, p_k are the basis functions for the boundary DOF. After the basic functions are found, the elementwise stiffness matrices and load vectors are found by integrating energy over the element volume and loads over the element boundary. The SimSolid solves the analysis problem in an iterative manner meaning the number of DOF is increased after each analysis pass. (Altair 2021.)

SimSolid can utilize most of the available 3D modeling file formats. Compared to the traditional FEA software's while using SimSolid, the part geometries can be imported as they

are without any requirement for making the parts or assemblies cleaner. Even the large assemblies can be imported to SimSolid as they are. SimSolid has a built-in feature to recognize part geometries such as bolts and utilize this data to further define the part assemblies on the model. This way, the SimSolid saves time and effort on the discretization of the analyzed structure. SimSolid is able to perform most commonly used analysis types such as structural static, dynamic and thermal analysis. The available dynamic analyses are modal analysis, transient and harmonic response. The damping can be given as modal damping ratio or Rayleigh damping. The harmonic and the transient analyses are based on the modal analysis so the modal analysis must be run before transient and harmonic response. Table 2 summarizes the main differences between SimSolid and the commonly used traditional FEA software. (Altair 2021.)

Table 2. Difference between SimSolid and traditional FEM

Property	SimSolid	FEM
Degree of freedom (DOF)	DOF is not associated points, but it is associated with surfaces.	DOFs are associated with nodes.
Meshing	No meshing to be done.	The user does the meshing after selecting the element type.
Elements	Volumes and surfaces are elements.	Elements type to be defined by the user.
Shape functions	Shape functions can be arbitrary classes and are derived during solving.	Shape functions define element property and affect the solution.
Geometry importing	Imported 3D models can and should be utilized as they are.	Models may require some simplification.
Geometry creating	Geometries can be modified or created. Assembly parts can be removed or suppressed.	Geometry for meshing can be generated in software.

From the analysis solving perspective, the big difference between the meshless SimSolid method and traditional FEM is the formation of the approximation shape functions. In FEM, the shape functions define the element properties that must be considered when choosing the element type. Choosing the element type in traditional FEM is based on the structure and the

expected results from the analysis. In the meshless methods and SimSolid methods the shape functions are based on the structure volume geometry. The approximating functions are based on the point scatter inside the structure's geometry. The SimSolid solver is iterating the solution on each so-called adaptive pass meaning that the density of point scatter increases at each pass where it is necessary. The traditional FEM has the mesh fixed when the analysis is run, and re-iteration of the solution requires re-meshing. The boundary conditions on FEM can be applied on each node and they can be set to constrain any translation or rotation possible. In SimSolid, the appliance of the loads and constraints is set on geometry faces, so in other words, the geometrical features affect the possible appliance of the boundary conditions. This background reflect well on how the SimSolid tool is intended to simulate complete design assemblies quickly.

The differences in how the geometry is treated make the SimSolid approach and traditional FEA software different types of tools for similar a goal. However, neither is redundant as they are optimal for different analysis situations. The SimSolid is most practical when the complete 3D model assembly is ready and static or dynamic loading case should be studied when the results are expected to be ready within days. The FEM is more suitable for more detail-oriented studies where the outcome of results is intended to be controlled carefully. The computational accuracy of the dynamic analysis is discussed in the benchmarking chapter.

2.3 Structural Dynamics

Structural dynamics is a field of study that focuses on structures or machines response to the time-varying load for which most of them are subjected in their life cycle. The motivation for analyzing the dynamics of structures is to avoid harmful excitations, increase their performance while dynamic excitations are applied and increase their life cycle.

There are various reasons why the structures and machines are being designed and manufactured lighter. The drawback of making structures lighter is that they are more

sensitive dynamic excitations. The motivation for performing the case studies in this thesis comes from the need to analyze the dynamics of a lighter structure.

Any structure like a bar under axial loading can be seen as a spring as its analytical solution for axial displacement can be derived into spring stiffness. The same method for defining spring stiffness can be utilized for other structural or machine elements like beams and shafts. The key in dynamic analysis is to have the mass or inertia and stiffness defined. Knowing the stiffness and mass of the system we can set the equation for the natural frequency of the system followingly.

$$\omega_n = \sqrt{\frac{k}{m}} \tag{2.21}$$

The equation 2.21 could represent any single DOF system with a mass and a spring stiffness. The result of equation 2.21 is a natural frequency of with unit is rad/s (Inman 2013, p. 9). The relationship between natural frequency and the frequency is described by equation 2.22

$$f_n = \frac{\omega_n}{2\pi} \tag{2.22}$$

The frequency as defined by the equation 2.22 could be explained as how many vibration oscillations occur per second. The inverse of the frequency is called period. The period describes the length of oscillation peak-to-peak time.

2.3.1 Dynamic Analysis

FEA software has built-in codes for running the dynamic analysis of the structures. The three common dynamic analysis types are modal analysis, harmonic analysis and transient analysis. One of the main differences in dynamic analysis compared to the static case is that

a dynamic analysis also includes a global mass matrix of the structure constructed of each element's mass matrix.

A harmonic analysis provides steady-state solution to the response of the system to structure under oscillating harmonic load. The harmonic analysis depends on the structure's natural frequencies and the frequency and amplitude of the applied load. Solution of harmonic analysis will provide magnitude of displacements, velocities and the accelerations at each node of the structure. The results are examined in a steady-state solution where the magnitude of the desired output is shown with respect to selected frequency range. This steady-state solution is useful in the design phase, showing the harmful frequencies which should be avoided. (Mac Donald 2011, p. 257.)

The transient analysis provides a solution as a function of time. The transient analysis is useful when the structure is subjected to a multiple load cases such as time dependent and harmonic loads. Solving the transient solution requires solving the time dependent equation of motion. The FEA software use methods of numerical time integration to solve the displacement at given time steps. (Mac Donald 2011, p. 259.)

In the meshless methods, the overall procedure of solving dynamic problems is similar to traditional FEA. With meshless methods, like in mesh-based FEM modal and forced vibration analyses like transient and harmonic response can be carried. The global stiffness matrix and the stiffness matrix are formed from the local domain matrices in the meshless methods. In these cases, local domains are utilized depending on the type of meshless method. Like in mesh-based FEM, the global matrices are used for solving the dynamic problem. (Liu 2018, p. 255-258.)

The mass matrix of the element can be defined knowing the matrix of shape functions. With the stiffness matrix, the shape functions are used to form the strain displacement matrix, but with the mass matrix, the material properties and shape functions are utilized followingly. (Rao 2018, p. 458.)

$$\mathbf{M}_{\mathrm{e}} = \int \rho \mathbf{N}^T \mathbf{N} dV \tag{2.23}$$

The matrix obtained by the equation 2.23 is the so-called consistent mass matrix. It is called consistent because the displacement approximations are utilized as on the stiffness matrix. For the meshless methods, the mass matrix can be formed similarly by utilizing the shape function matrices obtained by interpolation methods like the moving least square method (Liu 2010, p. 258.). The matrix containing only diagonal terms can be utilized too and is called lumped mass matrix. The lumped matrix assumes that each degree of freedom has concentrated mass affecting them. The lumped matrices are sufficient enough for computational accuracy and offer a possibility to reduce the computational speed. (Singiresu 2018 p. 459-460). But the lumped matrices can produce computational errors if the elements have a rotational degree of freedom like in the case of beam elements. (Inman 2013, p. 638.)

2.3.2 Natural Frequencies and Mode Shapes

The modal analysis is useful for determining the natural frequencies and their mode shapes of the structure. The modal analysis is a useful tool for determining harmful excitations to the structure and at which node or location of structure these excitations should be particularly avoided. Unlike in the static case the modal analysis, the modal analysis does not require any constraints on the structure as the solution is obtained from the eigenvalue problem containing mass and stiffness matrix. (Mac Donald 2011, p. 255-256.)

The natural frequency determined in Equation 2.21 is suitable for single mass and spring system with one deformation. However, in many analyzed systems there are multiple moving bodies and harmful resonances may occur at multiple different locations at different frequencies. The systems having multiple moving bodies are called multi-degree-of-freedom (MDOF) systems meaning that while analyzing them more than one degree of freedom must be considered.

The modal analysis of MDOF systems begins with constructing a mass and stiffness matrix of the system. The size of both mass and stiffness matrix depends on the degrees of freedom of the system. The eigenvalues and eigenvectors are obtained by solving an eigenvalue problem in Equation 2.24. (Inman 2013, p. 311.)

$$(-\omega_n^2\mathbf{M} + \mathbf{K})\mathbf{u} = 0 \tag{2.24}$$

The eigenvalues obtained represent the natural frequencies ω_n of the system. The number of obtained natural frequencies depend on the system's degrees of freedom, as the size of these matrices depends on the system's degrees of freedom. The matrix of mode vectors $\mathbf{u}$ is solved for each solved eigenvalue ω_n^2 like the eigenvectors in the eigenvalue problem. Each mode vector represents relative displacements of the system at each natural frequency that the system is vibrating at.

Systems that are under-constrained will have a so-called rigid body modes. The natural frequency is zero at these modes and the there is no relative displacement between systems nodes. This means that the system is moving as a whole rigid body. Rigid body mode can also occur when the system is constrained by flexible supports such as very soft springs. The system translates as one body supported by or multiple springs in these cases. The modes that produce deformations are usually referred to as elastic modes.

The eigenvalue problem is quite simple to solve if the system consists of two degrees of freedom as it results in two natural frequencies to be obtained. Moving to a higher number of degrees of freedom, solving eigenvalues becomes more complicated. Most of the available engineering mathematical tools such as MATLAB are able to calculate the eigenvalues and vectors by simple code (Newland 1989 p. 122-123). In the FEM codes, the eigenvalue problems are solved by various numerical methods. These available methods are the Lanczos method or other iterative methods like inverse iteration. (Liu 2010, p. 22.)

2.3.3 Harmonic Response Analysis

A harmonic response results from structures being subjected to harmonic periodic loading. Such excitation may occur to structures from any kind of rotating machinery, such as pulleys, fans and rotors. A typical commonly known issue of harmonic response is an out-of-balance car wheel that is balanced by adding extra weight on the rim. (Inman 2013, p.118). The harmonic response can be divided into two parts a transient and a steady-state. The transient response occurs at the start of the motion caused by a forced response. Once the transient vanishes, the steady-state response is left. In harmonic response analysis, the interest is in the steady state as the aim is to study systems that are subjected to forced vibrations at a constant excitation frequency. (Braun, et al. 2002, p. 1293.)

The harmonic response is caused by the forcing frequency and the amplitude of the applied force. The forcing frequency can also be called input, driving or forcing frequency. The driving force of the harmonic response is defined by Equation 2.26. (Inman 2013, p.119.)

$$F(t) = f_0 \omega t \tag{2.26}$$

The amplitude caused by harmonic excitation can be calculated by Equation 2.27. The Equation 2.27 is for undamped systems with one degree of freedom. (Inman 2013, p.120.)

$$O = \frac{f_0}{\omega_n^2 - \omega^2} \tag{2.27}$$

The harmonic response can also be solved for MDOF systems. The equation of motion for the multiple degrees of freedom system subjected to a harmonic forced response can be set as in Equation 2.28. (Inman 2013, p. 119.)

$$\mathbf{M}\ddot{\mathbf{x}}(t) + \mathbf{K}\mathbf{x}(t) = \mathbf{F}(t) \tag{2.28}$$

The Equation 2.28 is used further to solve the amplitudes caused by forced excitations. The amplitudes are solved for each degree of freedom of the system. Typically, the amplitude is introduced as displacement and its derivatives. Knowing the amplitudes at each driving frequency yields a steady-state response. The closer the driving frequency gets to the natural frequency the higher the amplitude gets. This phenomenon is called resonance and is what the harmonic response analysis aims to find. With systems that don't have any damping the amplitude should be unbound according to equation 2.27. Real life systems however do have damping so in practice, due to harmonic excitation the responses amplitude peaks when the driving natural frequency gets close to one of the systems natural frequencies. For the damped MDOF system, the amplitude of each degree of freedom for each driving natural frequency can be obtained by equation 2.28. (Braun, et al. 2002, p. 1296.)

$$\mathbf{O} = (-\omega^2\mathbf{M} + i\omega\mathbf{C} + \mathbf{K})^{-1}\,\mathbf{F}_0 \tag{2.28}$$

In Equation 2.28, **C** is the damping matrix. In the damped MDOF system, the matrix of amplitudes $\mathbf{O}$ contains imaginary parts. The vector of amplitudes contains the responses to amplitudes of each degree of freedom and can be plotted against the driving frequency to obtain the systems steady-state solution.

The resonance condition of the system can be harmful and is usually avoided by various means. In the MDOF systems the resonance condition is not as simple as with single-degree-of-freedom. The MDOF systems have a natural frequency associated to each degree of freedom, meaning the systems response has as many resonant frequencies as it has degrees of freedom. (Inman 2013, p. 366-367.)

The resonance is controlled in systems design by various methods. The resonance amplitude can be reduced by applying damping to the system. The natural frequency can be shifted away from each other's by adjusting the system or moving the driving frequency. Vibration

absorbers can also reduce the vibration energy and hence, the vibration amplitude. With the utilization of vibration absorbers or a good isolation design the amplitude of resonance can be reduced. (Braun 2002, p. 1296.)

3. Benchmarking

The benchmarking is done for the SimSolid to understand how well the SimSolid can be applied for dynamic analysis by performing modal analyses in different studies. In this study four different structures are considered. Two similar beams with the same cross-sections but different span and boundary conditions, and two plates with different dimensions and similar boundary conditions.

The analyses are done using FEMAP FEA-software and SimSolid. All of the analysis cases are compared to the analytic solutions found in the literature. Analyses done in this benchmarking study are dynamic modal analyses. The modal analysis in FEMAP is set to Lanczos solver with the consistent mass matrix.

3.1 Methods

This chapter introduces the geometries, material properties and boundary conditions for the FEMAP and SimSolid analyses. Also, the equations used to form the closed-form solution are introduced.

In both FEMAP and the SimSolid analysis, a similar 3D geometry was imported while analysing the beams. In FEMAP, the mesh consisting of plate elements was done completely in the software, and for the SimSolid, the plate model was imported as a 3D geometry.

3.1.1 Materials, Geometry and Boundary Conditions

All materials used in these benchmark studies were isotropic materials with a linear material model. The material properties are shown in Table 2 below.

Table 2. Material properties used in the benchmarking studies

Material property	Value
Density [kg/m^3]	7820
Young's modulus [GPa]	210
Poisson's ratio	0.29

The considered beams were solid rectangular beams. Their cross-sectional dimensions were the same, but they had different lengths. The dimensional details of beams are shown in Figure 10.

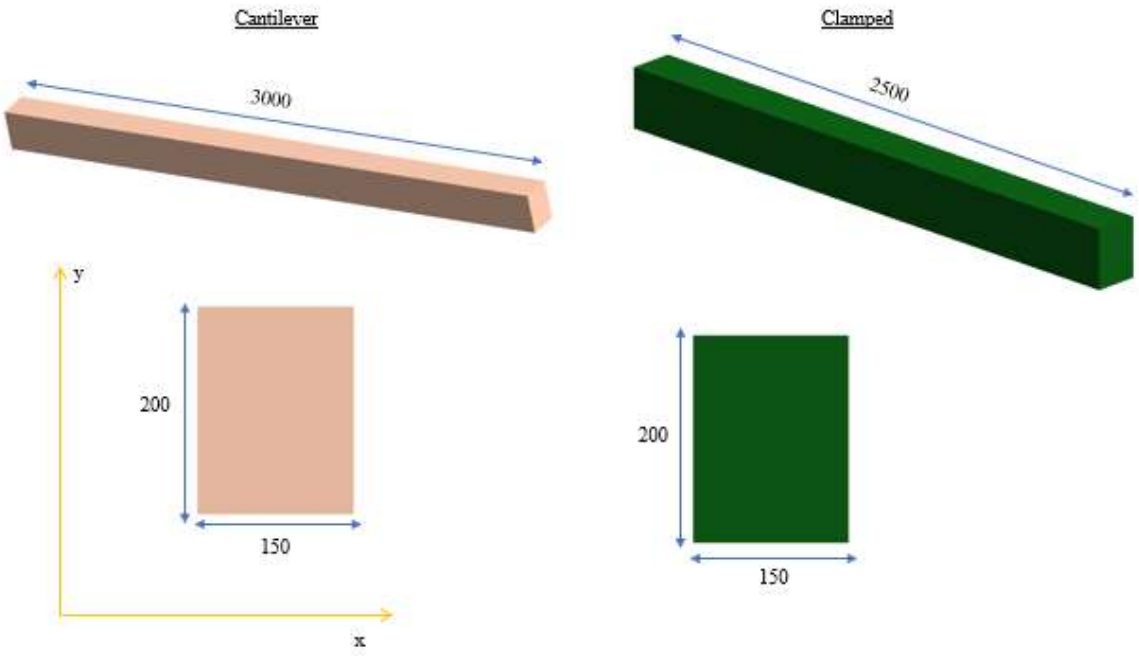

Figure 10. Dimensional details of the analysed beam.

The beams had the same cross-section but different spans and different boundary conditions. The cantilever beam had a fixed end free end. The fixed end means that the translations and rotations are constrained, and the free end allows both translations and rotations. The clamped beam had both of its ends fixed.

The plates had different thicknesses and dimensions widths, and heights but similar boundary conditions. The dimensions of plates that were analysed are shown in Figure 11.

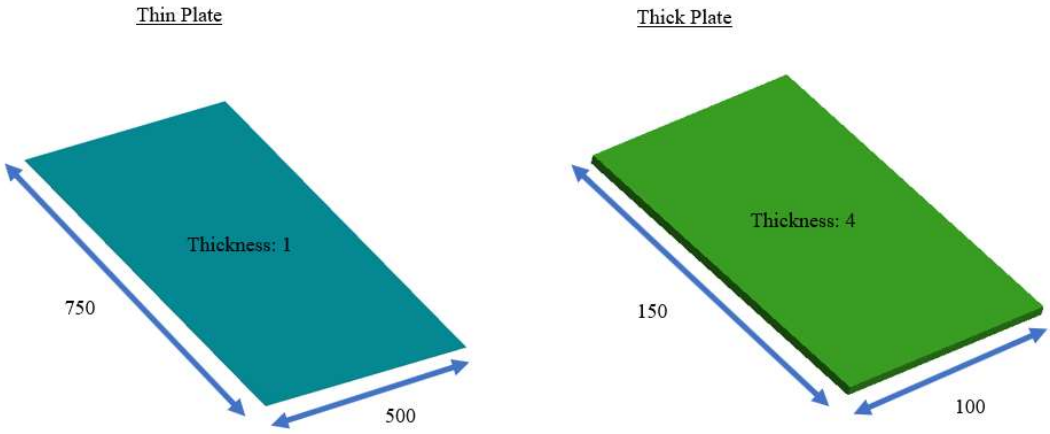

Figure 11. Plates that were analysed.

The dimensions and the boundary conditions of plates and beams are listed in Tables 3 and 4.

Table 3. Dimensions and boundary conditions of the beams.

Beam	Height [mm]	Width [mm]	Span [mm]	Boundary Conditions	Number of Elements (FEMAP)
Cantilever beam	200	150	3000	Cantilever fixed - free	3500
Clamped beam	200	150	2000	Fixed - fixed	1368

The mesh generated of the 3D models of beams on FEMAP consisted of 3500 elements for cantilever beam and 1368 elements for clamped beam. The number of elements increased to the level when the FEMAP model would converge. As the SimSolid utilized the meshless method no mesh was generated on the SimSolid.

Table 4. Dimensions and boundary conditions of plates.

Plate	Height [mm]	Width [mm]	Thickness [mm]	Boundary conditions	Number of Elements (FEMAP)
Thick Plate	150	100	4	Clamped on all edges	23500
Thin Plate	750	500	1	Clamped on all edges	15000

The decision of the ratio between height and width for the plate elements was based on available closed-form solutions for the natural frequencies of the plates. The FEMAP mesh contained 23500 plate elements on thick plate model and 1500 plate element on the thin plate. The FEMAP solver was set to utilize a consistent mass matrix. The SimSolid analyses were done with the solver being set to adapt to stiffness with four iterative passes.

3.1.2 Natural Frequencies of Beams and Plates

The closed-form solution for obtaining the natural frequencies of beams can be derived from the beam bending theory. The beam theory assumes a parabolic shape deformation for the beams and utilizes to material properties to form a beam bending formula. The modal solution for beams is based on a total of four different boundary conditions, free which allows translations and rotations, pinned which allows rotations, guided that allows for displacement but no rotation and clamped which fixes the beam end in terms of rotations and translations. The equation 3.1 is used to determine the natural frequencies of beam. (Blevins 2016, p. 134–137.)

$$f_{nb} = \frac{\lambda_i^2}{2\pi L^2}\sqrt{\frac{EI_y}{m_u}} \tag{3.1}$$

Where λ_i^2 is the dimensionless natural frequency parameter (of ith mode) and m_u is the mass per unit length of the beam (ρA). The natural frequency parameters depend on each set of boundary conditions.

The natural frequencies of beams are an increasing semi-infinite series. The term I_y is the second moment of inertia in the y-direction, so the results are obtained for natural frequencies of modes that deform in this direction. The orientation of the beam's cross-section is shown in Figure 10. Each successive mode has approximately one or half-wave more than the previous mode. Parameters for both boundary conditions set are listed in the table 5. (Blevins 2016, p. 138.)

Table 5 natural frequency parameters

Parameter	Cantilever	Clamped
λ_1	1.87510407	4.73004074
λ_2	4.69409113	7.85320462
λ_3	7.85475744	10.9956079
λ_4	10.99554073	14.1371655
λ_5	14.13716839	17.2787597

The parameters are substituted into Equation 3.1 to obtain five flexible natural frequencies of the beams.

The closed-form solutions for the natural frequencies of plates are based on the plate flexure theory. The theory assumes that the peaks of the deformed parts are assumed to be straight like the undeformed regions. Also, the bending stresses and the strains are proportional to distance from the mid surface. In the plate theory, there are three boundary conditions. Free allows rotations and translations, simply supported allows rotations but fixes translations and clamped fixes rotations and displacements. (Blevins 2016, p. 205.)

Like in beam cases, the natural frequencies of each mode are calculated utilizing a natural frequency parameter. This parameter depends on the boundary conditions and plates height to width ratio. The natural frequencies for plates can be obtained as followin. (Blevins 2016, p. 216.)

$$f_{np} = \frac{\lambda_{ij}^2}{2\pi a^2}\left[\frac{Et^2}{12\rho(1-v^2)}\right]^{\frac{1}{2}} \tag{3.2}$$

The dimension that relates to the geometry of the plate are a which is the plates longer edge and t that is the thickness of the plate. The material properties in Equation 3.2 are ρ material density, v Poison's ratio and E Young's modulus. The natural frequency parameters for clamped plates are listed in the following table. (Blevins 2016, p 216.)

Table 6 natural frequency parameters for clamped plates height to width ratio 1.5.

Parameter	Value	Mode Sequence
λ_1	60.77	1
λ_2	93.86	2
λ_3	148.8	3
λ_4	149.7	4
λ_5	179.9	5

In the case of plates, each natural calculated natural frequency corresponds to its own mode sequence. Different mode sequences have different number of waves produced in that mode in both horizontal directions. The plates considered in this study produce at most three waves and no more than two simultaneously in both directions. (Blevins 2016, p 216.)

3.2 Results

This chapter introduces the results of the modal analysis. The results are listed in the tables where the FEMAP and SimSolid results are compared to the closed-form solutions.

3.2.1 Beams

The natural frequencies for beams analysed on FEMAP and SimSolid are introduced in the table in Appendix 1. In total, there were 20 modes obtained from the analysis. The high number of modes is to elastic modes of the beams acting on both cross-sectional axis of the beams, meaning similar mode shapes are acting in two directions but with different natural frequencies due to different stiffness respect each cross-sectional axis.

The closed-form solutions and the modal analysis of the solid element beams can be compared only within those modes that correspond to the closed-form solution's described modes. The natural frequencies that are compared correspond to the modes 1-5, where the beam is deforming in the y-direction. Tables 7 and 8 show a comparison between FEMAP, SimSolid and closed-form solutions.

Table 7. Comparison of natural frequencies for cantilever beam

Mode	SimSolid [Hz]	FEMAP [Hz]	Beam equation 3.1 [Hz]	Difference FEMAP-Closed-form	Difference SimSolid-Closed-form
1	18.568	18.589	18.603	0.07 %	0.19 %
2	114.043	114.180	116.581	2.06 %	2.18 %
3	309.810	310.215	326.429	4.97 %	5.09 %
4	583.080	583.925	639.671	8.71 %	8.85 %
5	919.757	921.218	1057.421	12.88 %	13.02 %

Similar comparison table is arranged for the clamped beam.

Table 8. Comparison of natural frequencies for clamped beam.

Mode	SimSolid [Hz]	FEMAP [Hz]	Beam equation 3.1[Hz]	Difference FEMAP-Closed-form	Difference SimSolid-Closed-form
1	251.589	252.451	266.339	5.21 %	5.54 %
2	645.660	648.368	734.175	11.69 %	12.06 %
3	1168.727	1174.189	1439.277	18.42 %	18.80 %
4	1777.317	1785.918	2379.197	24.94 %	25.30 %
5	2444.001	2455.434	3554.110	30.91 %	31.23 %

The mode shapes of each corresponding natural frequency are shown in the figures below. Figure 12 shows the modes shapes for the cantilever beam and the Figure 13 for the clamped beam. These figures also include mode shapes computed by a closed-form solution (Steinberg 2000, p.63).

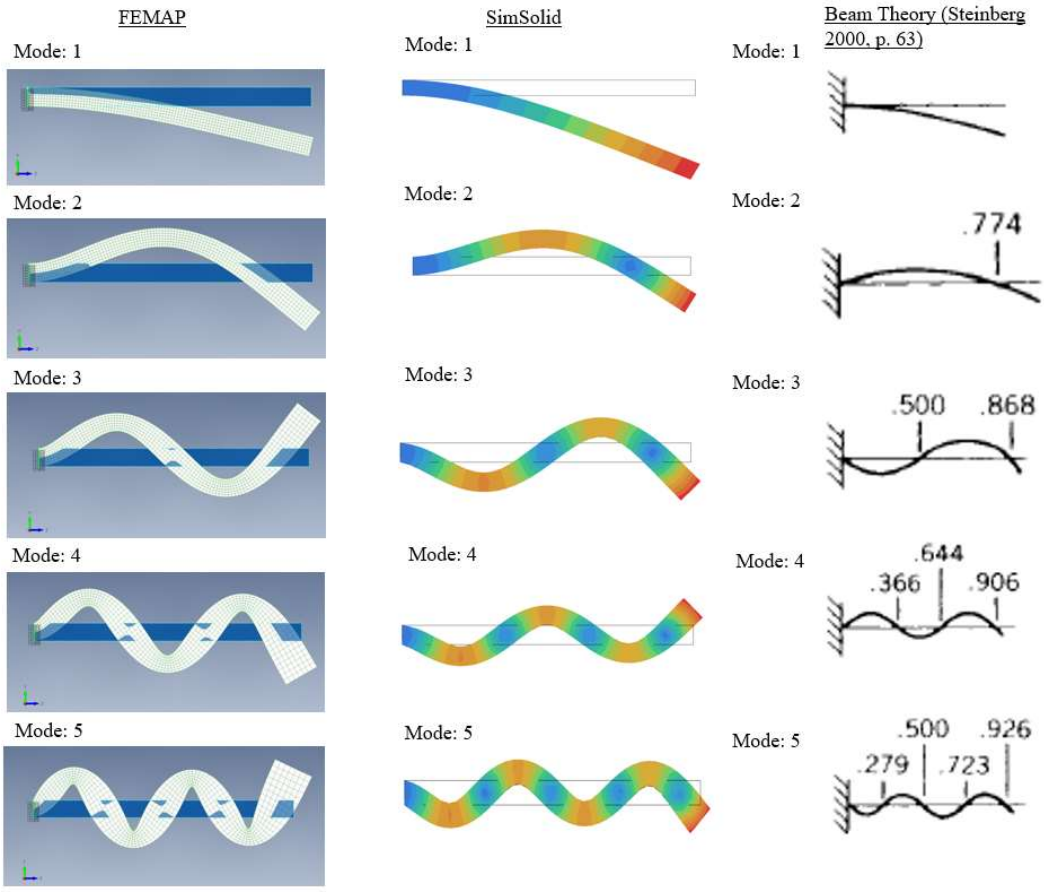

Figure 12. Mode shapes of the cantilever beam

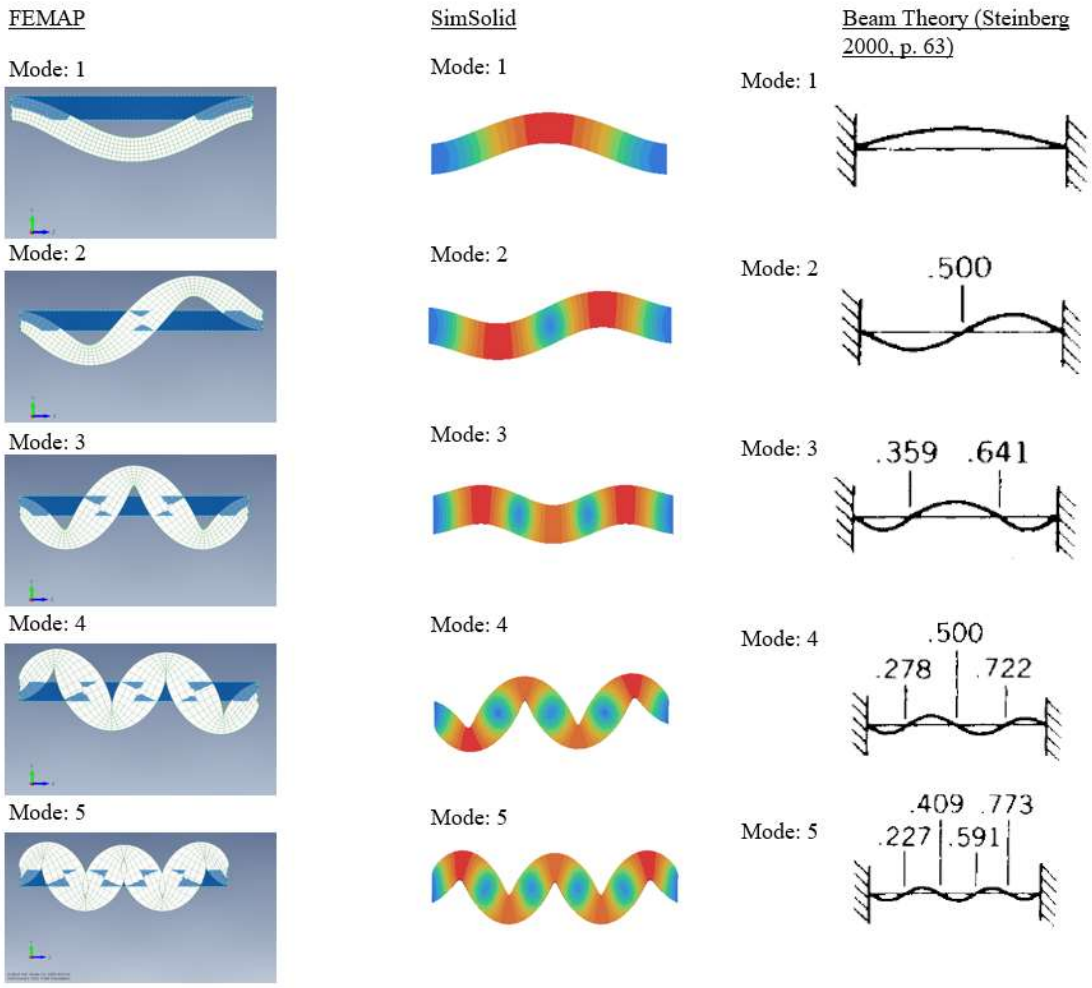

Figure 13. Mode shapes for clamped beam.

3.2.2 Plates

The number of natural frequencies obtained from the plate analysis is the same as the closed-form solution. The natural frequencies and comparisons are listed on the table 9 for the thick plate.

Table 9. Natural frequencies and their comparison for the thick plate.

Mode	SimSolid [Hz]	FEMAP [Hz]	Plate Equation 3.2 [Hz]	Difference FEMAP-Closed form	Difference SimSolid-Closed form
1	2655.091	2652.670	2688.686	1.34 %	1.25 %
2	4073.503	4078.120	4151.163	1.76 %	1.87 %
3	6409.196	6413.644	6581.004	2.54 %	2.61 %
4	6443.764	6462.889	6620.808	2.39 %	2.67 %
5	7692.475	7707.329	7948.624	3.04 %	3.22 %

Table 10. Natural frequencies and their comparison for the thin plate.

Mode	SimSolid [Hz]	FEMAP [Hz]	Plate Equation 3.2 [HZ]	Difference FEMAP-Closed form	Difference SimSolid-Closed Form
1	26.802	26.868	26.877	0.03 %	0.28 %
2	41.303	41.485	41.512	0.07 %	0.50 %
3	65.605	65.786	65.810	0.04 %	0.31 %
4	65.810	66.168	66.208	0.06 %	0.60 %
5	78.867	79.369	79.476	0.14 %	0.77 %

The mode shapes for the thick plate are shown in the Figure 14 and the thin plate in Figure 15.

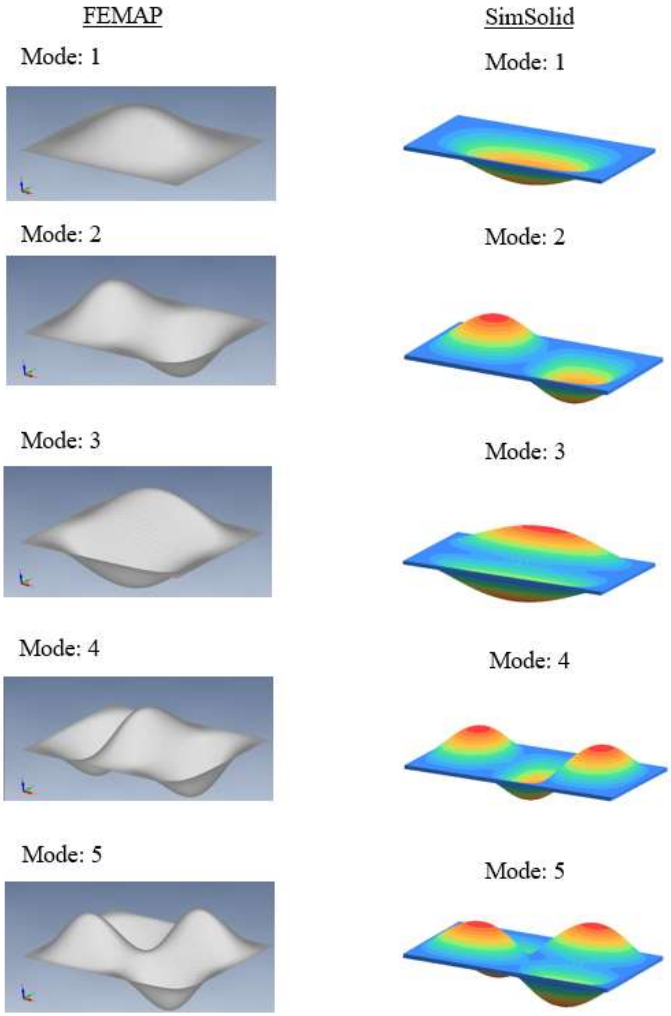

Figure 14. Mode shapes of thick plate

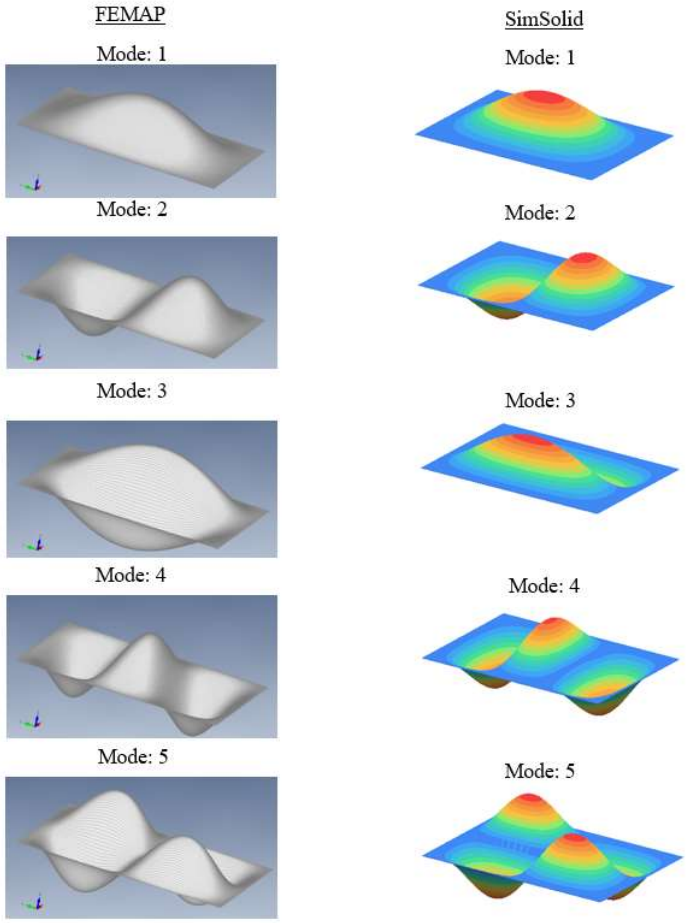

Figure 15. Mode shapes of thin plate.

3.3 Discussion

The natural frequencies for both plate and beam cases were similar in magnitude. In all cases, the difference compared to closed-form solution was high when comparing the results of higher frequencies. Only in the thin plate case all the obtained natural frequencies were within close range. In beam cases, the number of obtained modes was high, but it was still possible to obtain the similar modes than could be expected from the beam theory. Figures 12 and 13 show comparable modes shapes between FEMAP, SimSolid and closed-form solution.

In the case of beams, the difference in higher frequencies can be said to be because of the nature of solid elements. In higher frequencies, the solid elements mode shapes showed

deformation also in the element cross-section. Figures 12 and 13 show that the beam deformation at those analysed modes was similar, but in the higher frequencies, modes 4 and 5, the beam cross-section experiences significant deformation. The solid elements can deform within their cross-section, unlike the beam elements that are not deforming along their cross-section. SimSolid does not utilize the element-wise discretization, but similar mode shapes were obtained from modal analysis. Looking at the natural frequencies of each natural frequency in the Appendix 1 for SimSolid and FEMAP, it can be noticed that the natural frequencies' values were of similar magnitude.

The SimSolid performed well in the first three natural frequencies for beams and plate in low frequencies. In higher frequencies the deviation from the closed-form solution was larger for FEMAP too. The NAFEMS has benchmarked SimSolid with a thin cantilever plate that produces low natural frequencies, the accuracy was similar to the thin the thin plate in this benchmarking study (Altair 2018). It is also possible that if the beam structures studied in this bench marking study were slender beams, the results would match more closely to the close form solutions as they matched in the thin plate case.

Also, benchmarking done by Liu showed that the other meshless methods provide similar accuracy in dynamic analysis. He analysed beams with the meshless Local Petrov-Galerking method and ABAQUS FEM software. In his results, the difference between natural frequencies is larger for the larger frequencies. According to these results, the difference can be mitigated by having a finer FEM (and meshfree) model with a higher number of nodes (Liu 2010, p.260-261).

This study did benchmarking with a larger scope for both beam and plate cases. The benchmarking results show that the results of the dynamic analysis done by SimSolid are relatable to the analysis done in a traditional FEM approach like FEMAP, where the plate and solid elements were used. In the case of beams, the solid elements and SimSolid's meshless approach can be compared to the closed-form solution in lower frequencies. In higher frequencies the deviation can be higher depending on the beam size and applied boundary conditions. In the case of plates, the larger the magnitude of the obtained natural

frequency gets, the larger deviation is. For the FEMAP analyses, the convergence was insured by refining the mesh. This technique corresponded to SimSolid's feature of adaptive passes. In future it, would also be worth studying how SimSolid's results would compare when setting adaptation from stiffness to stress or when changing the number of adaptive passes.

4. Case Studies and Results

The case studies were done on a whole elevator car system. The system under investigation was the whole assembly that included the elevator car, car frame and car doors. The model used in the simulation was almost complete 3D assembly model, expect some minor parts like washers were removed. Also, the roller guides were removed to apply proper boundary conditions.

The ride quality impact was examined on the harmonic response analysis. In the Meshless model, the harmonic response analysis was linked to the modal analysis for the 100 modes. All the analyses were done with the linear material model. The analysis methods and results are introduced furtherly.

The results were validated on the actual prototype elevator doing ride quality measurements during the elevator run. The measurements were obtained by EVA measurements, placing the measuring instrument at the middle of the elevator car during the elevator run to measure physical car movements.

The overall process of the analyses can be summarized followingly. The modal analysis is performed on the whole system. The harmonic response analysis based on the modal analysis is performed to obtain the steady-state solution of the response of the system. The harmonic response analysis is done by simulating forced excitations coming from hoisting ropes to the pulley beam. The arbitrary load magnitude is selected as the actual exciting force is unknown. The harmonic response analysis indicates the most harmful frequencies causing resonance that can be measured at the middle of the car floor. The load is selected to act vertically as the main interest are vertical vibrations caused by excitations in vertical direction. The mode shapes are then examined to note how the structure behaving at those harmful frequencies. The potential design improvements are then validated, to test if the ride quality can be improved.

4.1 Boundary Conditions

The main boundary conditions are set on the simulation model at roller guide shoes and the rope support locations. Both were simulated as springs with spring stiffness corresponding to the actual physical part deflection. In the SimSolid model, these springs are set as virtual connections called grounded bushings. Figure 16 represents a free-body diagram of the elevator car system.

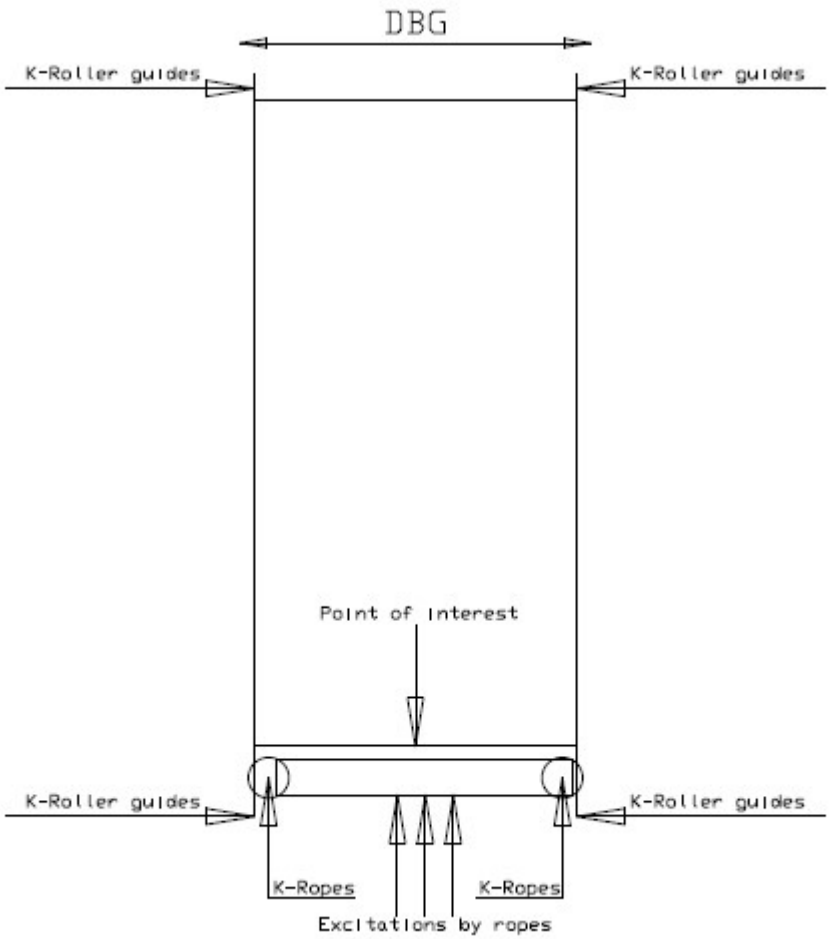

Figure 16. Free body diagram of the elevator car system.

In Figure 16, the k-ropes represent the constraints applied to simulate the rope supports. Similarly, the k-roller guides stand for the roller guide constraints.

The applied stiffness coefficient of the roller guides was based on the known stiffness value that has been measured on the deflection test. The rope stiffness can be defined in a similar way than it would be defined to a bar that is subjected to axial loading. The axial deformation of an axially loaded bar can be calculated using Equation 4.1.

$$x = \frac{NL}{EA} \tag{4.1}$$

Where the *N* stands for the normal axial load, now in order to get the spring stiffness, we need to set the *N/L* on the right-hand side of the equation so that Equation 4.1 will be in the following form.

$$k = \frac{EA}{L} \tag{4.2}$$

The assumption is that the elevator car system is most sensitive at the middle of the shaft when the elevator has reached its nominal speed. The bar length in Equation 4.2 can be considered as the travel of the elevator. The elevator car system is considered most sensitive in the middle of the elevator travel. So, the equation for the stiffness provided by a suspension ropes is defined as following.

$$k_{rp} = \frac{2EA}{H} \tag{4.3}$$

The actual stiffness term EA includes the stiffness of all the hoisting ropes combined. The value is based on the laboratory test. Stiffness, system parameters and material details are introduced furtherly.

4.2 Materials and System Parameters

Most of the system's structure was considered to be steel with few exceptions. Another applied material was the Cellasto which is a polyurethane polymer. The Cellasto is applied to the car frame isolation pieces and on the fixings of the pulley beam. (BAFS 2021)

Table 11 below shows the material properties and the system parameters that in the simulation.

Table 11. Materials and their properties

Parameter	Value
Steel density	7100 kg/m^3
Cellasto density	500 kg/m^3
Steel young's modulus	200 GPa
Cellasto young's modulus	1 MPa
Steel poisons ratio	0.29
Cellasto poisons ratio	0.05
Elevator travel	33.75 m
System mass	702 kg
Roller Guide stiffness, k_{rg} (in both directions)	$250 \cdot 10^3$ N/m
EA of ropes	7490536 N
Damping Ratio	0.03

In the simulation parameters, the steel density is adjusted to meet the total mass of the system. The elevator travel is the same for the elevator that the result validations were done. The Cellasto has a low poisons ratio because it's expected to have small (less than 20%) deformations. As the Cellasto is a hyper-elastic material, its stiffness properties, the poisons

ratio depends on the load and the deformation to which it is subjected to. On the actual system, the deformation for the Cellasto is less than 20%. Larger deformations are constrained mechanically. On Figure 17, Cellasto's behavior under compression is described.

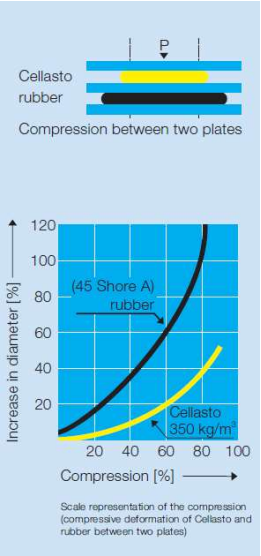

Figure 17. Cellasto behavior under compression (BASF 2021).

4.2.3 Load

In order to obtain the harmonic frequency response of the system a load of 10N is applied to the bottom part of the car frame pulley beam. In SimSolid the periodic load function was set to a constant load, so the loads amplitude function was constant.

The selection of the load magnitude is arbitrary because the target of the simulations is not to have exact quantitative values on the elevator car system response but rather indication on harmful excitation frequencies and their modes shapes. The load applied simulates the excitations coming from the hoisting ropes to the pulley beam of the car frame.

4.2.4 Analysis Cases and Settings

The case studies were carried out in five different case studies. The objective of the case studies is to compare different system configurations response. Additionally, the chosen case studies can provide ride quality improvement suggestions. Table 12 below shows all the analyzed cases.

Table 12. Case studies.

Case	Description
1	Base configuration
2	Roller guide spring coefficient 80%
3	Mass reduced
4	Car floor connections adjusted
5	Pulley beam fixing lever stiffness changed

The point of interest for results was selected at middle of the car floor. The location for the EVA measurement device during the ride quality assessment run that is used for validation is in middle of the elevator car floor.

4.3 Results

The results are obtained for the horizontal and vertical vibrations. The interest range for vertical vibrations is 0-100Hz and 0-20Hz horizontal because of how the humans perceive the in-car vibrations.

The horizontal accelerations are analyzed in two directions. These directions are side-to-side and in distance between guides (DBG) direction. These two directions are clarified on the horizontal view, Figure 18.

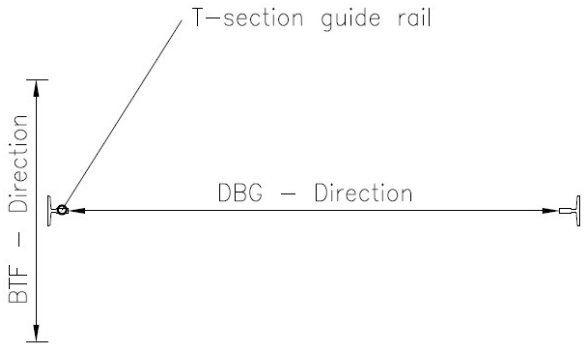

Figure 18. Horizontal directions at which the results are analyzed.

On the figure 10 the car guide rails are shown meaning that the DBG is the side-to-side respect to car and BTF is back-to-front.

4.3.1 Responses for Case 1 - Base Study

In the figures below, each of the results is shown. The first results are for the base study, Case study 1. Further results then show how the response changes when the configuration of the system is changed.

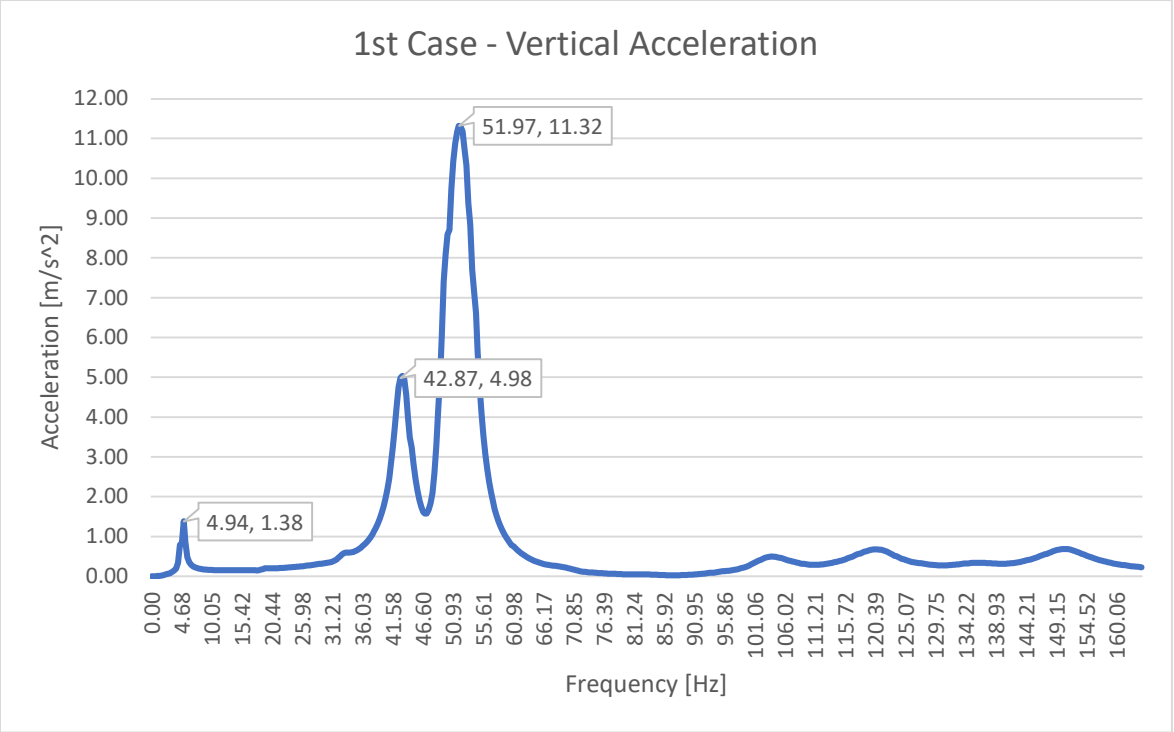

Figure 19. Vertical acceleration of the first case.

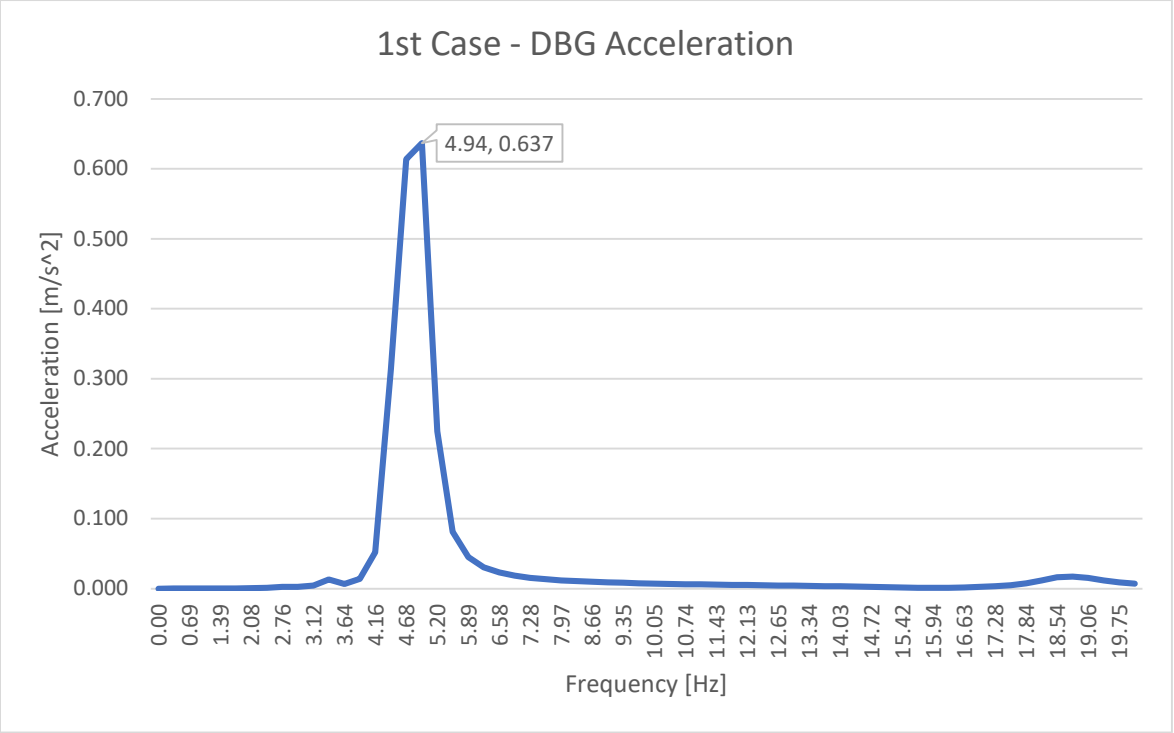

Figure 20. DGB acceleration of the first case.

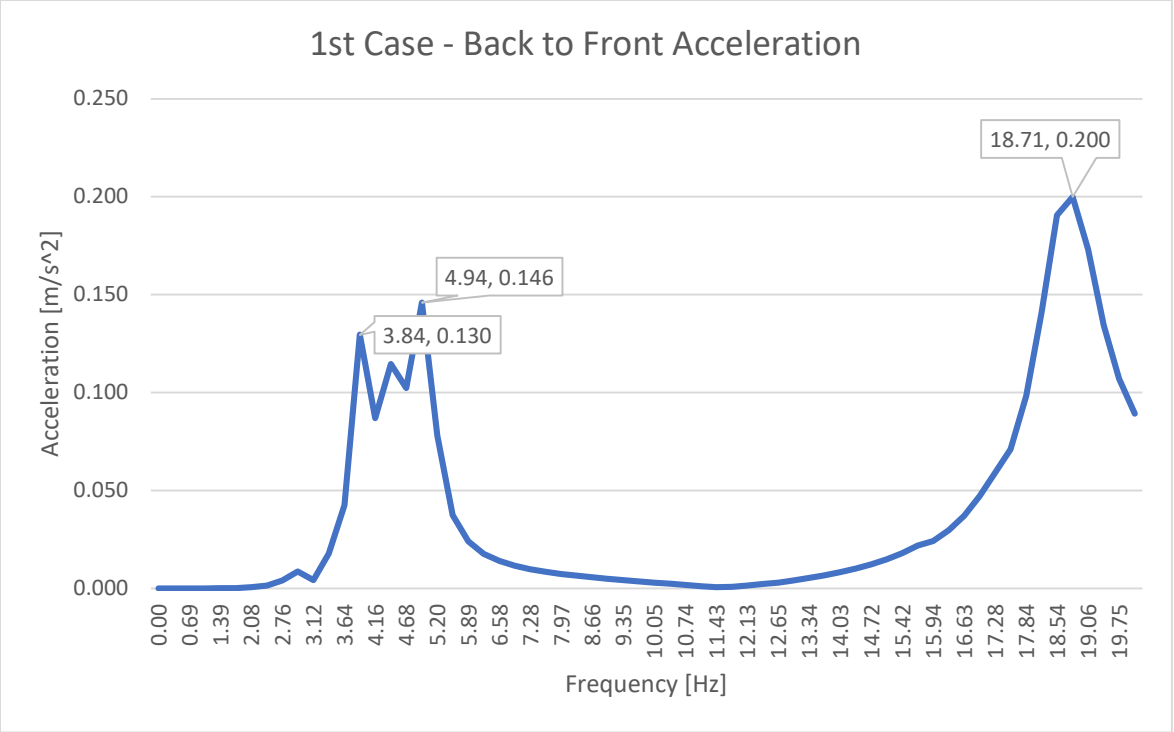

Figure 21. DGB acceleration of the first case.

From the figures above, it can be said that the system is most sensitive to vertical vibrations as the excitation load was set to act in vertical direction. The frequencies 43 Hz and 52 Hz cause the largest amplitudes in accelerations. Based on this simulation where the excitations are acting on the vertical direction the lateral vibrations were less significant but should have not been neglected in order to insure that there is no harmful response in horizontal directions.

4.3.2 Responses for Case 2 - Guide Shoe Stiffness

For the second case, the difference in the guide shoe stiffness is simulated. These responses simulate different guide shoe selections.

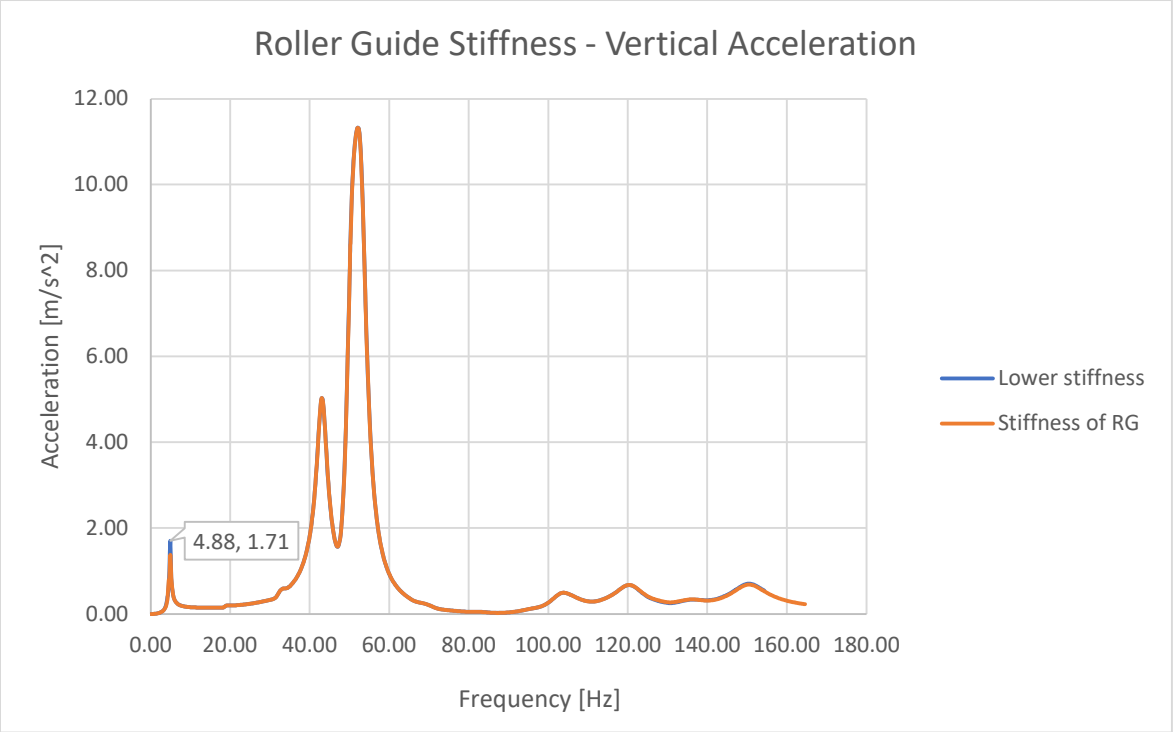

Figure 22. Vertical response with different guide shoe configuration.

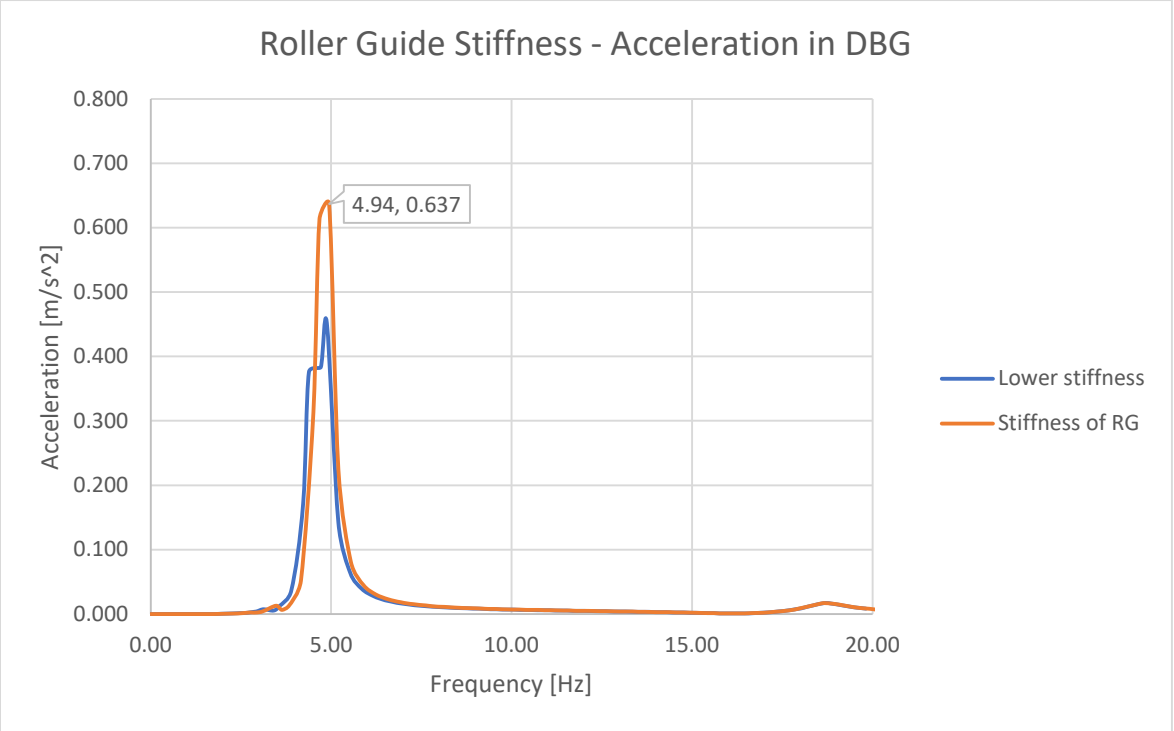

Figure 23. Response in DGB direction with lower guide shoe stiffness

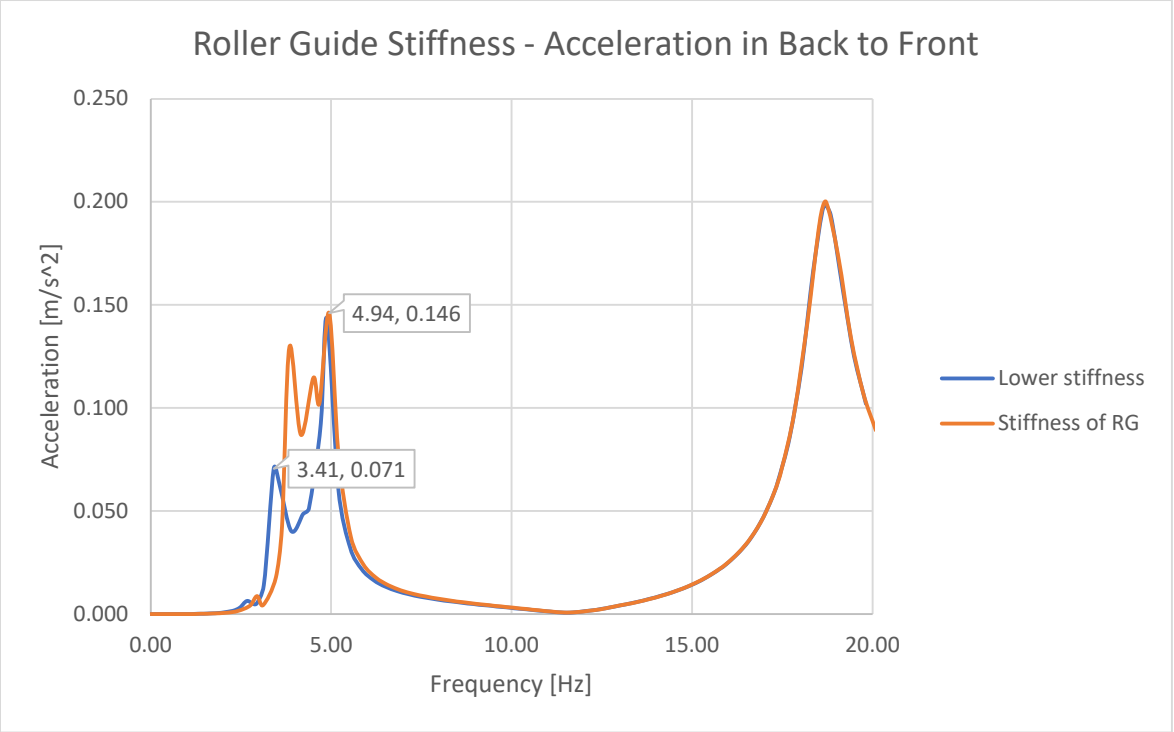

Figure 24. Response in back to front with lower guide shoe stiffness

The figures representing the response of the cases with lower guide shoe stiffness indicate that changing the roller guide type or material mostly affects horizontal vibrations. The vertical vibrations are only affected at lowest resonant peak. At this lowest resonant peak, the system experiences rigid body motion also in horizontal directions. This point can also be seen in responses of the lateral directions as the roller guide shoes' spring stiffness also contributes to that resonance. The responses acting in horizontal directions are nearly ten times lower than the vertical ones. This finding supports the assumption that the focus should be on vertical vibrations.

4.3.3 Responses for Case 3 - Response for Different System Mass

The following results were obtained to indicate on how the lower mass affects the dynamic response. The systems response with lower mass was studied in order to analyze the impact of lowering the car systems mass. Due to sustainability reasons, the elevator car systems mass can be reduced, but it makes it more sensitive to dynamic loadings.

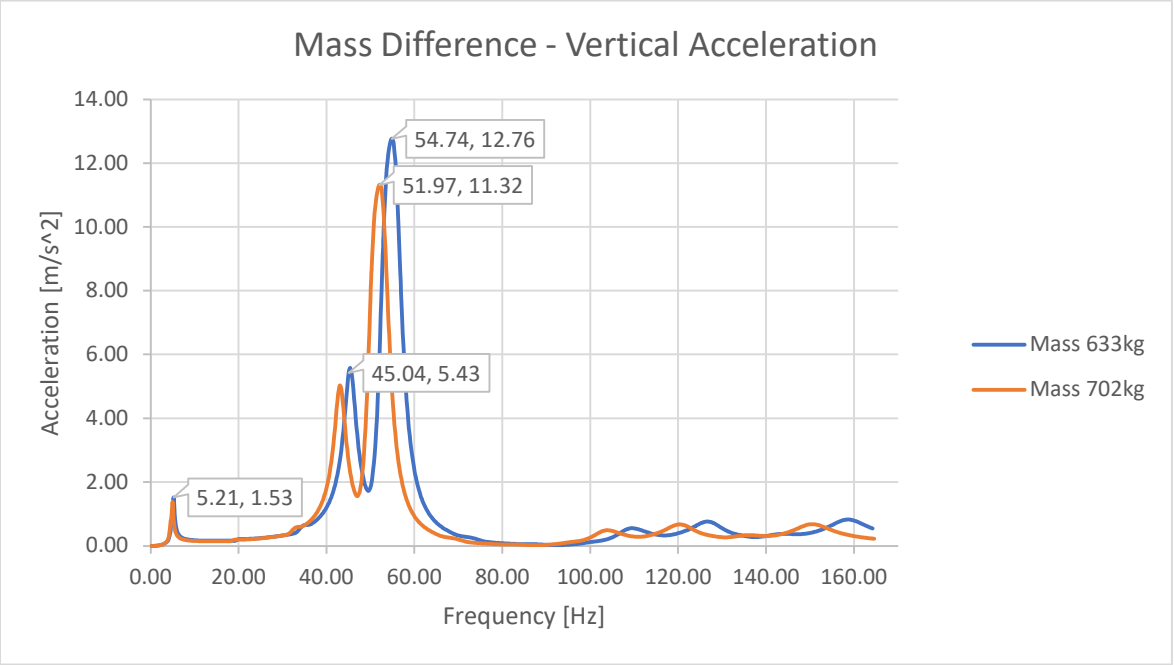

Figure 25. Vertical responses with different masses.

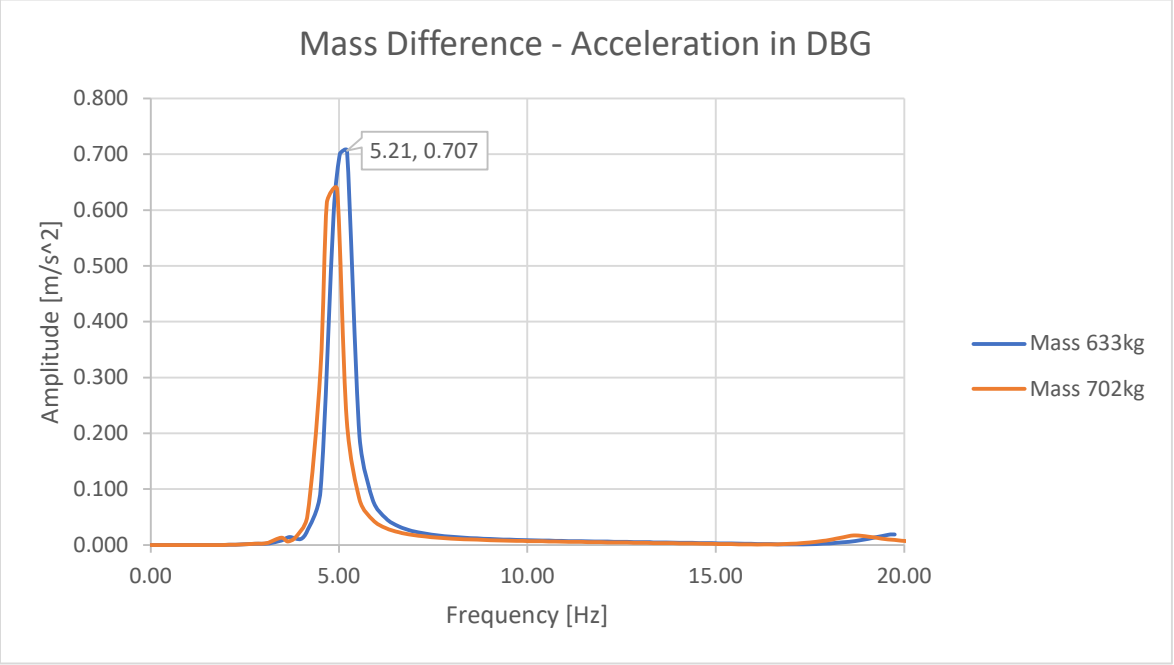

Figure 26. Horizontal response in DBG direction

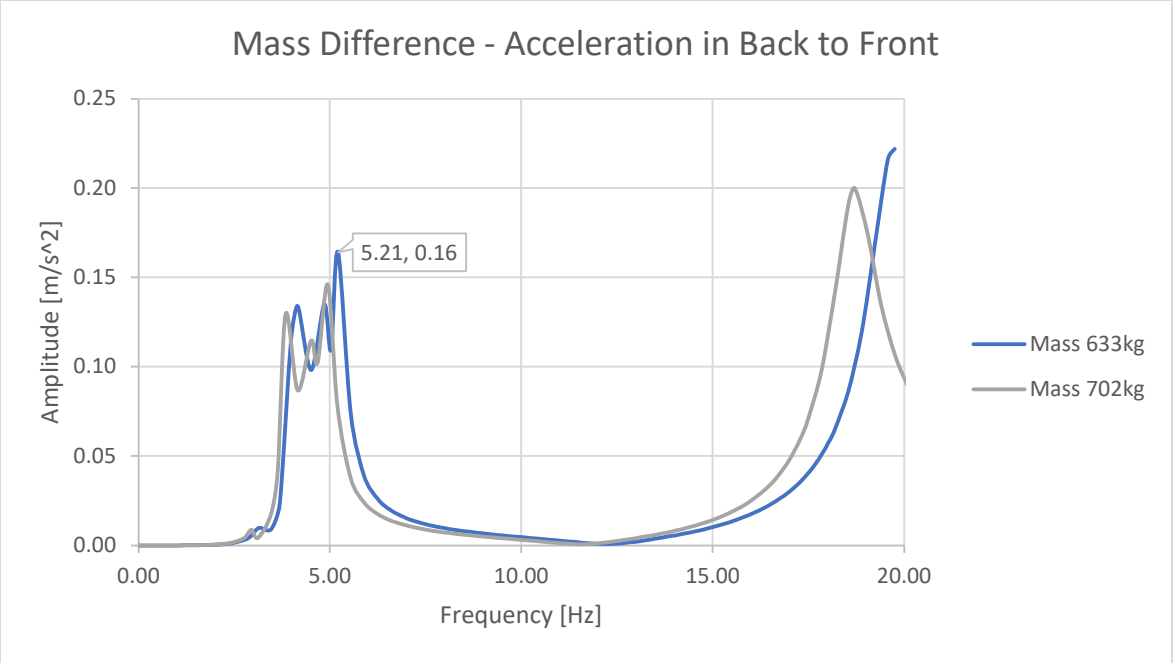

Figure 27. Horizontal response in back to front directions.

The 10% reduction in elevator car systems mass causes the amplitude at the peak vertical responses to increase by approximately 12% which is an expected outcome as the natural frequency of lighter structures is higher. This increases the risk of the vertical resonances being harmful to the elevator ride quality, but furtherly a means of mitigating this risk are introduced.

4.3.4 Responses for Case 4 - Car Floor Connection

The following case is analyzed to study the different impacts of the floor fixings. The reason to choose this approach is due the mode shapes of the first case. In these mode shapes the car floor was sensitive at its middle.

Intended fixings for the car floor were initially located on the sides of the car structure. The following simulations were ran with the floor being fixed from its stiffeners to the car frame beams. Figures 28, 29 and 30 compare the responses of the car floor being fixed from its stiffeners and being free. The free case in the Figure 28 is the base study.

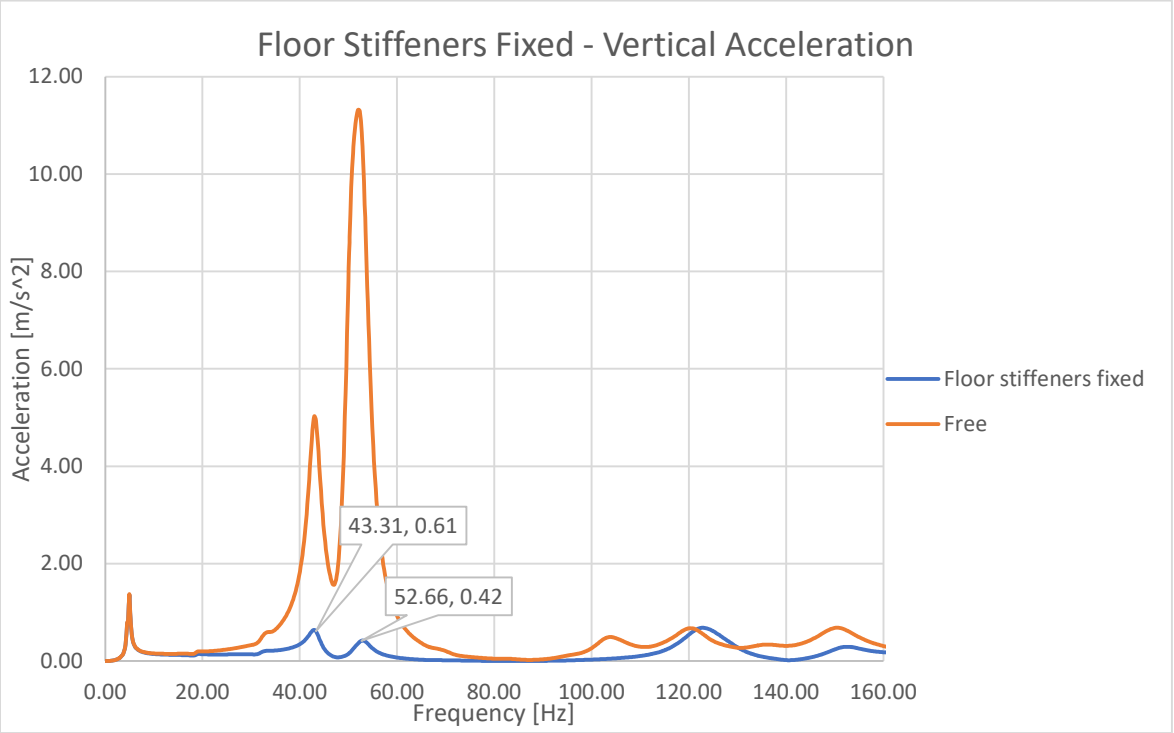

Figure 28. Comparing floor stiffeners in the vertical direction.

The difference between the floor being fixed instead of free is significant for the vertical vibrations because additional constraints are applied to the mid-car floor at the response measurement point. The constraint applied to the car floor mid-point does not allow the car floor to deform freely at the middle, so the resonance amplitude is much lower. Figures 29 and 30 are responses to the horizontal vibrations.

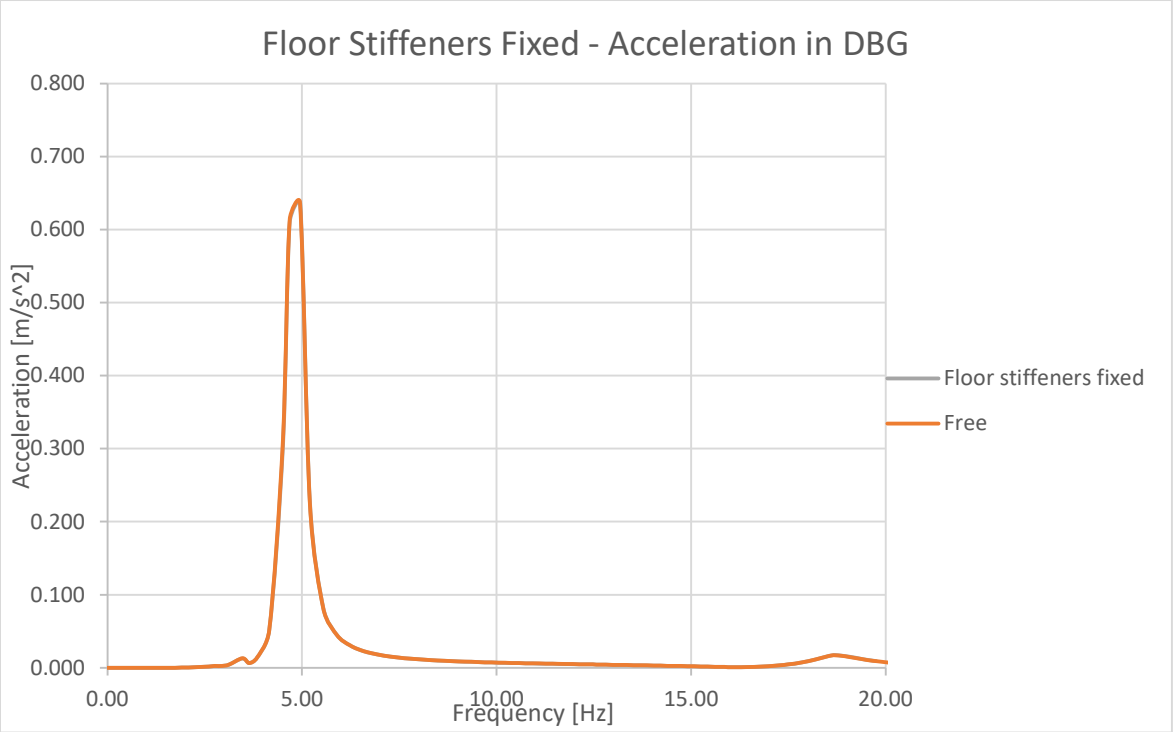

Figure 29. Changes in response for the DBG direction

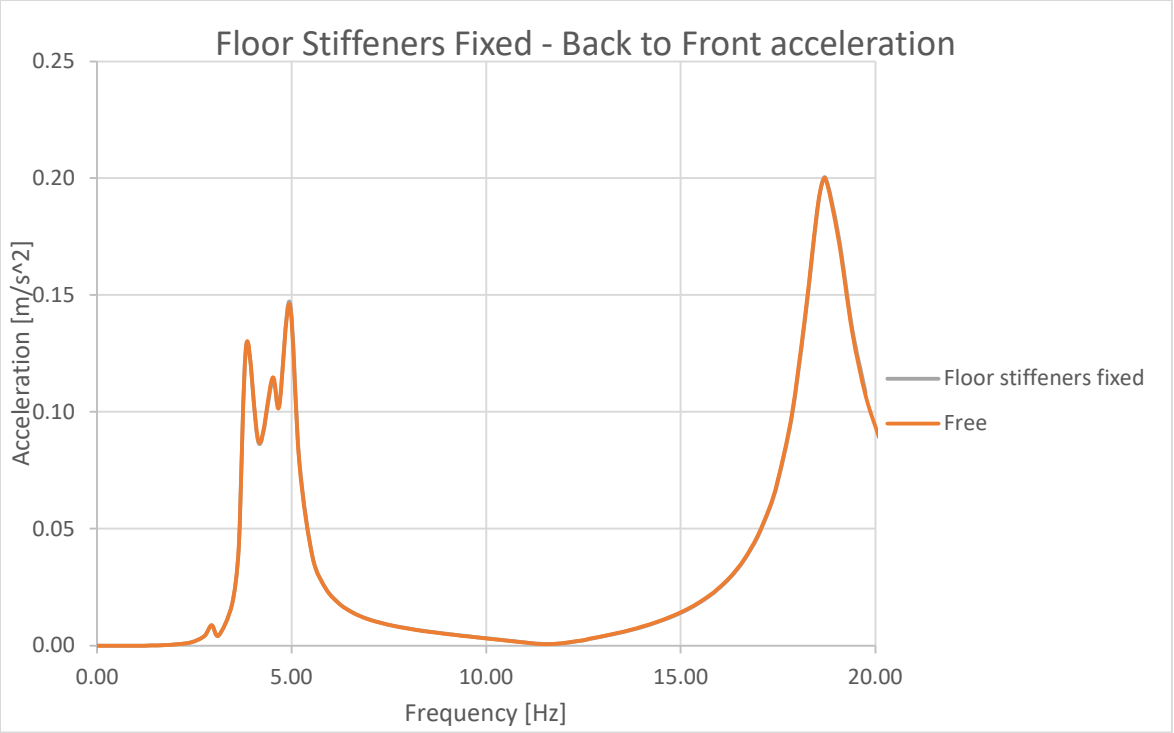

Figure 30. Response in back to front direction.

Changing the car floor constraint does not affect the horizontal vibrations. This outcome is expected because constraint applied to the mid-car floor should limit the vertical movement of the car floor.

4.3.5 Responses for Case 5 - Pulley Beam Fixings

The following responses were obtained for the different configurations for the pulley beam fixings. The cases were done with Cellasto stiffness increased to 1.5 MPa and with the plate material stiffness increased the 241 GPa. The pulley beam is fixed to the car frame beam via a lever with a couple of fixing details consisting of two plates and Cellasto pieces on the pulley beam and car frame beam side. Figure 31 shows the arrangement for the pulley beam fixing.

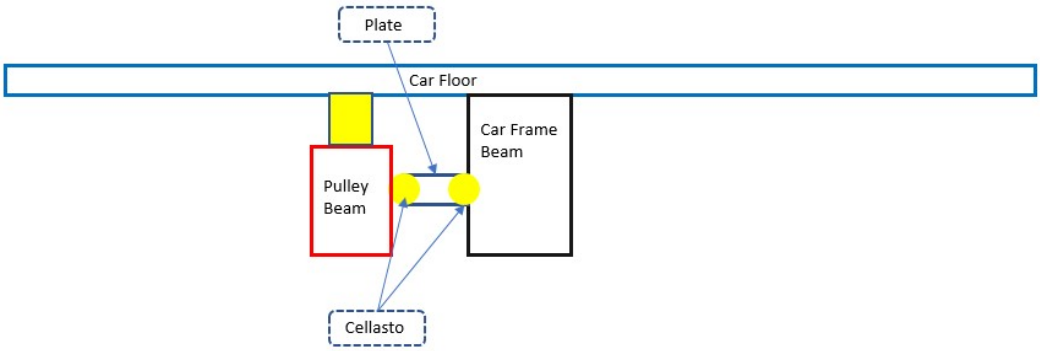

Figure 31. Pulley beam - car frame beam fixing details.

Figure 32 represents responses with different configurations of the Cellasto piece and the plate of the lever.

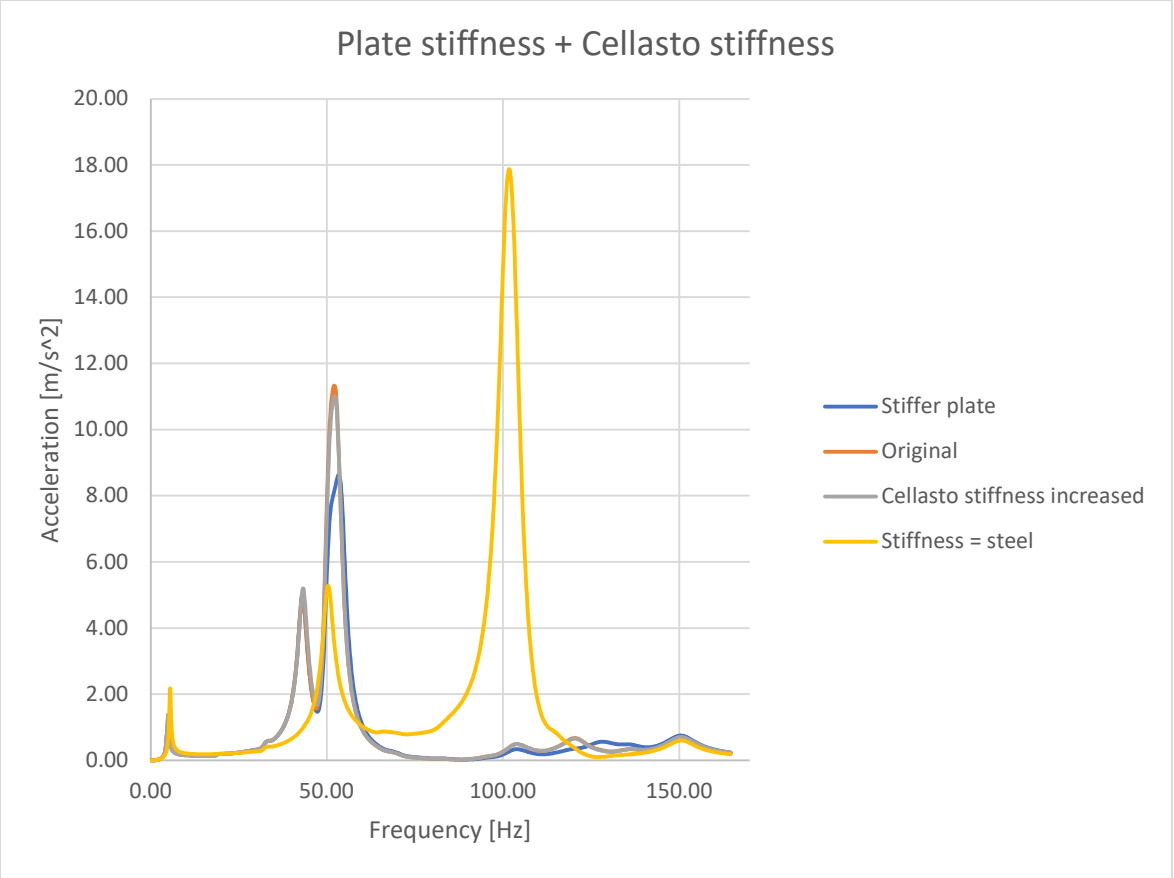

Figure 32. Response with different configurations of the pulley beam fixing details.

Considering Cases 1-4, vertical amplitudes cause the most impact on the systems response. Hence, the horizontal responses were not studied for the cases represented in the figure above.

4.3.6 Car Floor Fixing Study

As the case studies indicate, the biggest opportunity from the framework of the structural dynamics in improving the ride quality is the floor fixing method. In practice, the floor span should be reduced by fixing it on the car frame pulley beam approximately at the guide rail line. This finding was validated by performing additional measurements on the test elevator with having the floor fixed to the car frame beam by an angle bracket. Figure 33 represents the principle on how the angle bracket was fixed to the car floor and car frame structure.

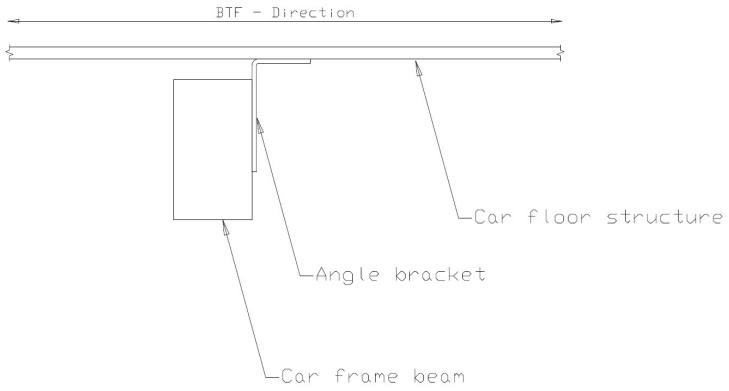

Figure 33. Angle bracket fixing to car frame beam and car floor structure.

The validation was done for both, with and without angle bracket to test the findings obtained from the dynamic analysis that indicates that the floor fixing can improve the dynamic performance of the elevator car.

4.3.7 Validation

The validation of the results was done on the test elevator with the EVA measurement device. The measurements were done by placing the EVA-625 measurement device at the centre of the car. The centre of the car is a similar location that was the point of interest on the dynamic analyses. Figure 34 represents the measurement arrangement inside the car.

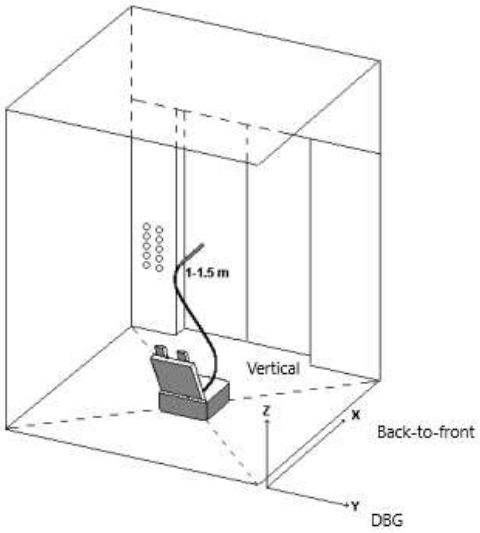

Figure 34. Measurement arrangement (PMT, 2018)

In Figure 34, the instrument location for the in-car noise measurement is also shown but it is not relevant for the in-car vibrations study. During the measurement runs, one person was present inside the elevator car.

The FFTs of the measured elevator runs are shown in Figures 35, and with assembly where the angle bracket was installed the analysis is shown in Figure 36. The FFT's shown in Figure 36 corresponds to the Case study 4, Figure 28. The FTT's were obtained from 16 seconds of the elevators nominal speed run. The results were obtained from both up- and downward runs meaning the measurement were taken from ascending and descending elevator.

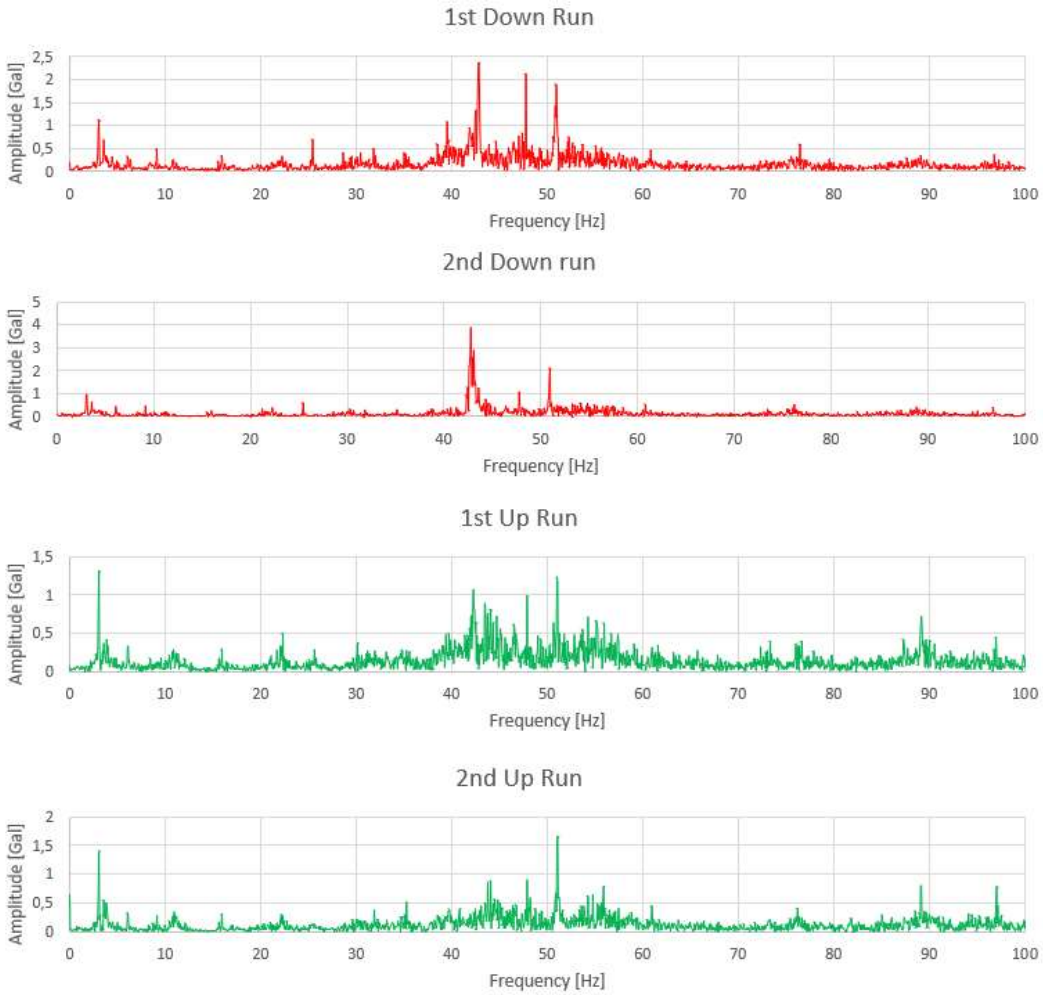

Figure 35. FFT of the measurements. Validation of the case 1.

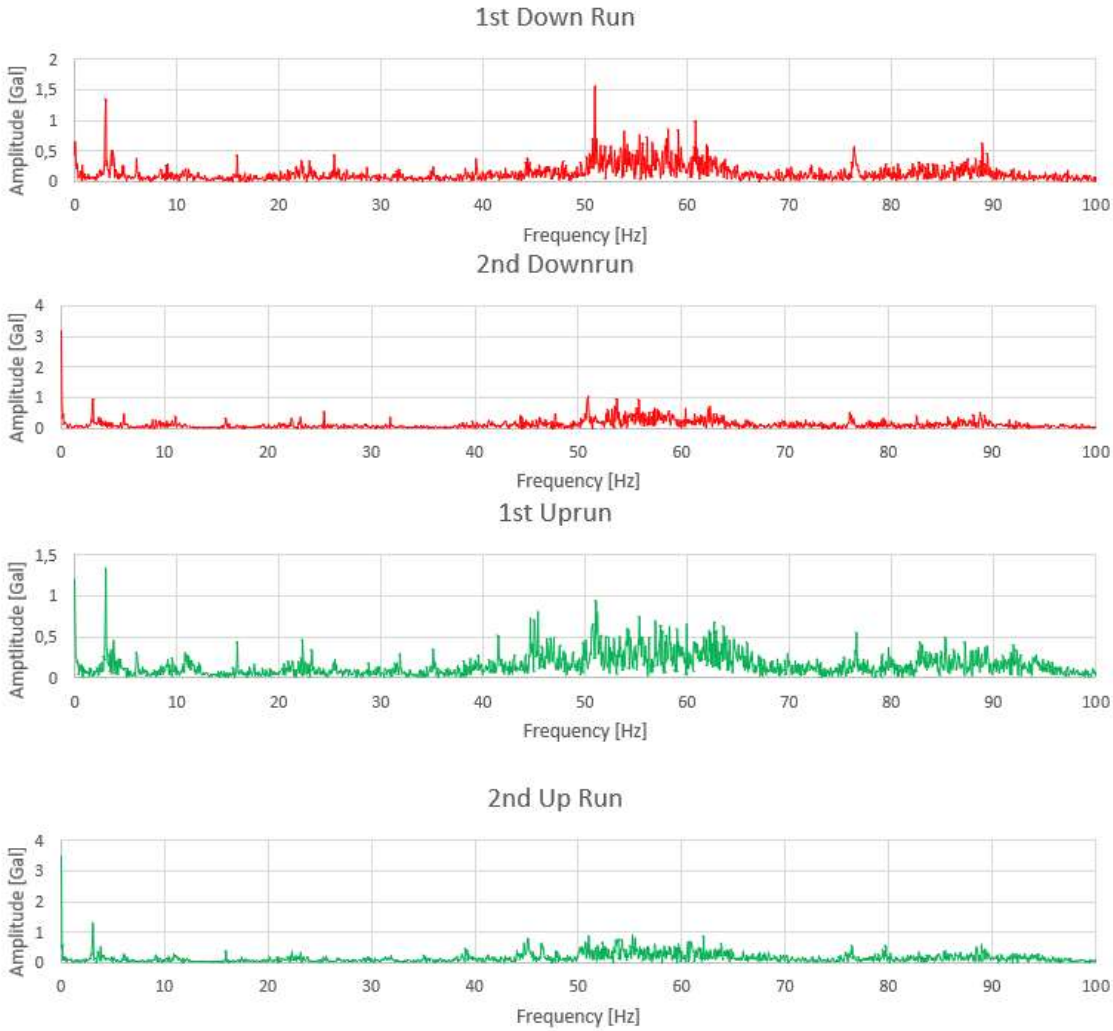

Figure 36. FFT of the measurements. Validation of the case 4.

The FFTs of the measurements show the peak frequencies during the elevator run. The peak frequencies at 60-61 Hz range and 3 Hz range are known to be the forced excitations caused by machinery and the pulleys. The rest are structural resonances that are excited by the hoisting ropes. The measurements in Figure 35, without angle bracket corresponds to the base case study. The peak frequencies that are seen in FFT figures are similar to the analysis case of the first case. Table 13 is summarizes the peak structural resonances of each run at three largest amplitudes.

Table 13. Frequencies causing peak amplitudes.

	Without Angle Bracket		With Angle Bracket		Simulated Case 1	Simulated Case 4
Run	Peak frequency [Hz]	Amplitude [Gal]	Peak frequency [Hz]	Amplitude [Gal]	Peak frequency [Hz]	Peak frequency [Hz]
1st Down	50.9	1.91	58.1	0.86	52	53
1st Down	47.8	2.14	59.1	0.84	43	43
1st Down	42.8	2.38	50.9	1.57	5	5
1st Up	51.0	1.23	55.3	0.75	-	-
1st Up	47.9	0.99	51.1	0.99	-	-
1st Up	42.3	1.07	45.4	0.82	-	-
2nd Down	50.9	2.09	55.9	0.95	-	-
2nd Down	47.8	1.10	53.8	0.97	-	-
2nd Down	42.8	3.91	50.9	1.03	-	-
2nd Up	51.1	1.66	55.3	0.89	-	-
2nd Up	47.9	0.91	51.0	0.88	-	-
2nd Up	44.1	0.89	45.2	0.76	-	-

Comparing dynamic analysis results of the first case it shows similarly that the peak amplitudes occur at the range of 40-52 Hz when validating the elevator without the angle bracket installed. There are few frequencies that cause peak amplitudes and are not visible in the analysis. These can be caused by the imperfections of the model compared to real assembly especially when considering the joints of the components as there might for example be loose connections between assemblies that are ideal in the model. The measurements of the cases with and without angle bracket are compared in Figure 37.

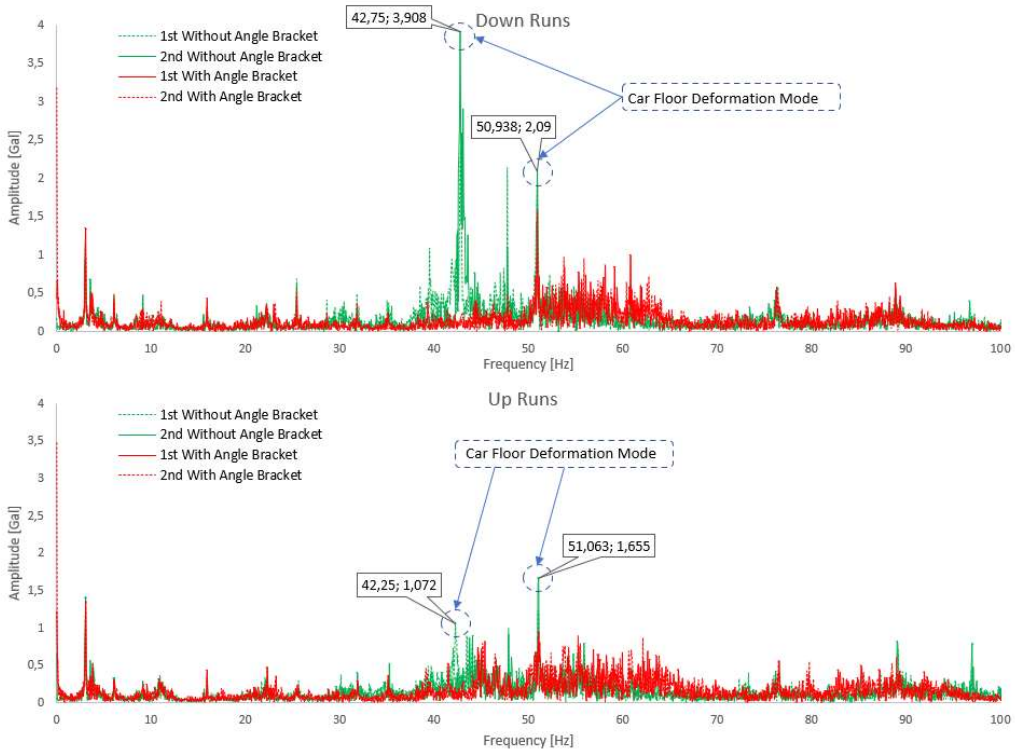

Figure 37. Comparison of the FFT's between runs with and without angle bracket.

On the figure 37 we can see that the measurements validate the natural frequencies at which the car floor is in resonance. These peaks 43 Hz and 52 Hz were also visible in the in dynamic analysis on figures 19 and 28, as listed on the table 13. However, the magnitude levels are different than on the analysed case studies. The comparison between measurements and the analysed cases is shown on the figure 38. The magnitudes of the amplitudes are not comparable between simulation and the measurements, but the amplitude trend and the resonance frequencies can be compared.

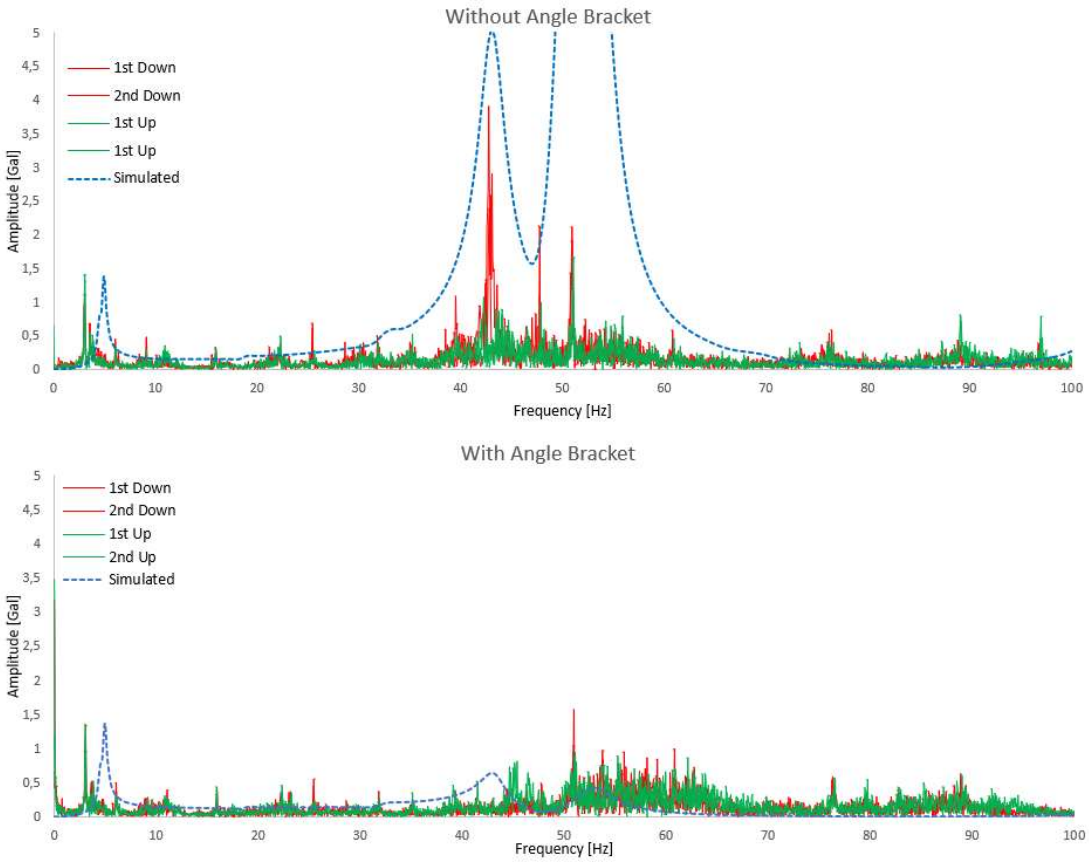

Figure 38. Comparison between the simulation and the measurements.

The simulation indicates that the 43 Hz peak is lower than the 52 Hz peak in amplitude, but the amplitude is higher at 43 Hz on the elevator down runs. This result is caused by a higher excitation force in the downwards runs. The dynamic analysis shows that the low-frequency resonance at 5 Hz should be causing a rigid body motion. On the measurements, the lowest peak is at the 3 Hz range and is actually caused by the rotating motion of the pulleys. The floor is now fixed to the car frame reducing its span, and the angle bracket itself is causing an impact on the response. If the additional mass of the angle bracket had caused a significant impact on the results, the frequency peaks would have been lowered as the natural frequency lowers when keeping the stiffness constant and increasing mass. It can be said that the fixings of the angle bracket by self-tapping screws are most likely causing the peak frequencies to be shifted higher. Also, the angle bar structure is causing a structural resonance area between 50-60 Hz. Simulating this behaviour may be a difficult task as boundary conditions for the angle bracket screw fixings would have to be modelled as accurately as possible.

The prototype testing with the angle bracket show promising results that reducing the floor span by fixing it to the car frame beam can reduce the peak amplitudes and thus improve the overall ride quality performance. The average peak values reduced from 1,7 Gal to 0,9 Gal, leading to a better ride quality.

All of the up and down runs were measured with similar measurement arrangement. Despite this, the measurements show some deviation on each run. The deviation occurred for both, peak frequencies and peak amplitudes. The deviations in the measurement are mostly caused by the elevator system that was measured instead of the measurement instruments. The elevator system that was investigated in these studies is very sensitive to the varying excitations coming from the electrical system and machinery. There are various reasons why the excitations deviate between the runs. The machinery operating temperature affecting the electrical system, is one of the reasons why the measured response is different between measured runs. During the elevator down runs the measured amplitude at the 43 Hz range was higher. Up and down runs result in different responses as the load seen by the motor is different due to balancing of the system with counterweight that is heavier than the car when there is only one person inside the car. Also, lifting and guiding arrangement of the car creates different friction forces when going up and down.

The test arrangement can be said to be identical between each test runs. However, as the test has been performed with a single person inside the elevator car, who was doing the measurements there are some factors affecting the responses. Placement of the measurement device is intended to be exactly at the middle of the car, but it's difficult to replicate this exact position. The biggest variation in response can be said to come from the position of the person who is standing inside the car during the run performing the measurements. The position of the person affects the whole elevator car systems stiffness, in the components fixings and the roller guides.

4.4 Discussion

Based on the simulation results and the validation, dynamic analysis done by meshless methods can be utilized for improving the ride quality of an elevator car. The analysis were done on multiple cases showing how the mass of overall system, different roller guide types and floor fixing affect the dynamic response. Case study 5 show that the pulley beam fixings affect the dynamic response. Considering the mode shapes of Case 1, the pulley beam and the car floor were sensitive at the 43 Hz and 51 Hz frequencies causing peak amplitudes.

The validation measurements show that the different floor fixing methods help improve the ride quality of the elevator car system. The FFT's of the EVA measurements show in quantities how much the peak amplitudes can be reduced. By reducing the peak amplitudes, the ride quality of the elevator car can be improved. The FFT's validate that the root cause of the peak amplitudes is the resonance of the car floor structure.

There were three peak amplitudes at the range of 0-100 Hz in vertical vibrations. The first peak is at the 5 Hz, which is close to the natural frequency of the whole spring mass- system where ropes support the whole mass of the system. Substituting the stiffness of the hoisting ropes and whole system mass to the following equation for obtaining natural frequency we get all most the similar value than the 5 Hz.

$$f_{rb} = \frac{1}{2\pi}\sqrt{\frac{k_{rp}}{m_{sys}}} \tag{4.1}$$

After substituting total rope stiffness and system mass, Equation 4.1 yields value of 4 Hz, which is not completely the same as the peak frequency value because the pulley beam is not completely centered respect to the car mid-axis. In analysis, this causes a mode shape where the car moves rigidly in vertical and horizontal directions. Figure 39 represents the mode shape at 5 Hz.

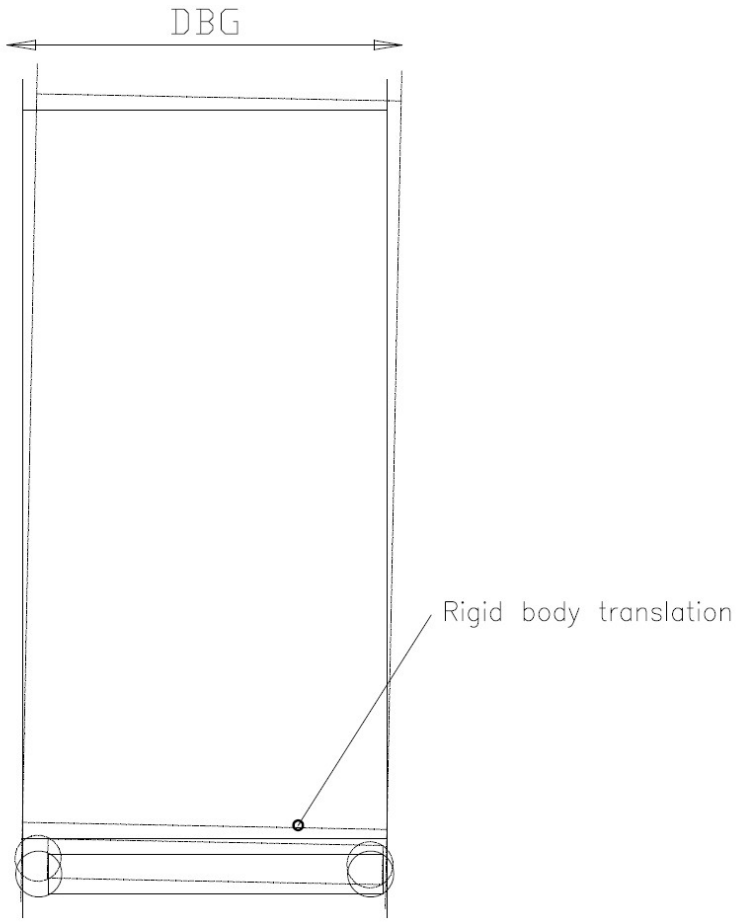

Figure 39. Rigid body translation at the 4.95 Hz mode.

In Figure 40, the vertical translation of the car occurs also within the horizontal axis too meaning, the spring supports that model the guide shoes also contribute to the stiffness of this particular mode. This peak frequency can also be seen in the results of both horizontal responses in Figures 20 and 21. These back-to-front and DBG movements are in horizontal directions because pulley beam is not centered on the car's middle axis. On the FFT of the back-to-front vibrations, in Figure 40 we can see this peak value approximately at this range. The presence of this peak value at this range also validates the assumption that the elevator car is experiencing most vibration movements in the middle of the travel. The mid-travel is also when the elevator is traveling at its nominal speed.

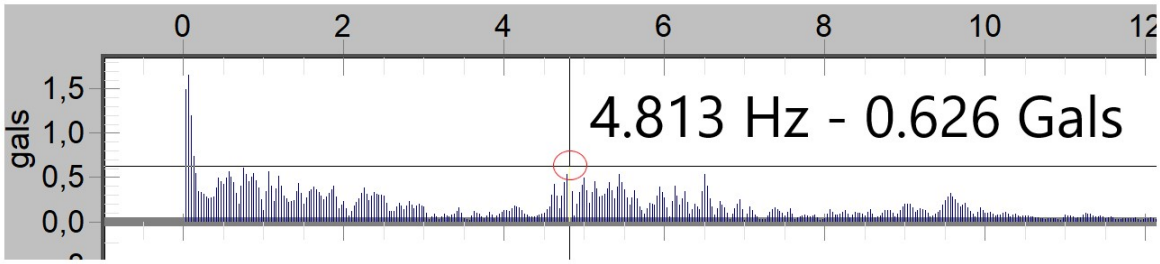

Figure 40. Peak back-to-front frequency.

At the peak frequencies 43 Hz and 52 Hz, Figure 19 indicates that these cause a resonance. The resonance occurs when the excitation frequency is close to the natural frequency of the mode at which the car floor is sensitive. Looking at the mode shapes at those particular natural frequencies, both the pulley beam and the car floor are deforming. Figure 41 represents the mode shapes of the car floor at these resonant two resonant frequencies.

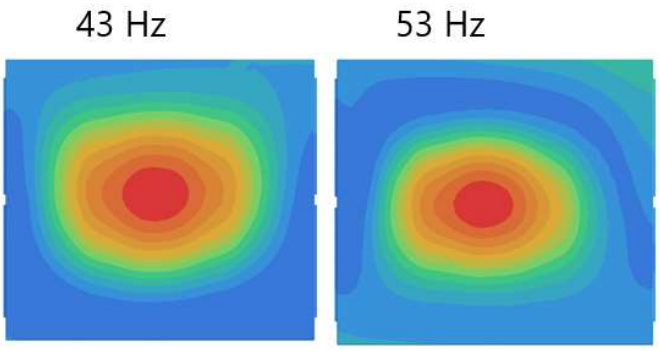

Figure 41. Modes shapes of car floor at natural frequencies 43 and 53 Hz from the top view.

These two mode shapes in the Figure 41 correspond to the closest natural frequency compared to the obtained resonant frequency. Figure 28 shows how the response amplitude is much lower than in the first analyzed case. In Case 4 the car floor movement was constrained by setting a fixed connection between the car frame beam and the floor. The amplitude peaks in acceleration are still present, but they are reduced significantly when the car floor is fixed in the middle.

When optimizing the dynamic behavior for structure under harmonic excitation, a common procedure is to is to shift the resonant frequency peak from the excitation frequency within a sufficient tolerance. Simplest of which is to tune the excitation frequency from the harmful range. In the case of optimizing the ride quality of the elevator car this, this frequency peak shift is not the ideal as the avoided excitations occur at wide range, 0-100 Hz in vertical and 0-20 Hz in horizontal. Another way of shifting the resonance peak is by applying additional damper mass or increasing the overall mass of the system. In the case of the elevator car, the appliance of extra mass is not feasible as this will affect overall components of the elevator the system. The effect of increasing moving masses of the elevator system will also increase the cost of the elevator system. The outcome proposal in these case studies is to affect the resonant frequencies amplitudes by changing the design of the structure's assembly.

5 Conclusions

The objectives of this thesis were to perform dynamic analyses using meshless method. Successful and validated dynamic analyses show that the meshless method can be utilized for improving the ride quality of the elevator car system. The dynamic analysis was used to find the most relevant modes that affect the elevator ride quality. Based on the results of the dynamic analysis, design improvements were proposed to improve the ride quality of the elevator car system.

The dynamic analyses were done for a whole 3D CAD assembly of the car system including doors, car frame and the car. The analyses done were: modal analysis of 100 modes and the harmonic response analyses. The results of the harmonic response analyses were obtained at the middle of the car floor. This approach simulated the car ride quality assessment where the car actual movements are measured by placing a measurement instrument at the centre of the car floor. The dynamic analysis indicated that the resonance amplitude could be reduced significantly by fixing the car floor at its middle to the beams of the car frame. The analysis results have been validated by measurements showing good accuracy between the analyzed and measured resonant frequency ranges. The overall method utilized for dynamic analysis in this thesis can be summarized followingly. First the eigenvalue analysis is required. After the eigenvalue analysis the structure is excited in desired directions in the harmonic response analysis. Based on these analyses the components sensitive to the excitations can be found by examining the mode shapes of the structure. After examining the mode shapes a design improvements can be proposed and validated by repeating the analysis with the proposed configuration. In addition, impacts of other configuration changes based on business or sustainability requirements for example lowering the friction by introducing different guide shoe configurations or reducing the weight of the system can be analyzed.

The dynamic analysis done in the case studies indicate that the most relevant nominal frequencies were 5 Hz, 52 Hz and 43 Hz. These were the peak frequencies obtained by the base study case. Both of the elastic nominal modes 52 Hz and 43 Hz the pulley beam and

the car floor experience deformations. The main design improvement proposed for the ride quality improvement is to provide an additional fixing for the car floor. This eliminates the mode shape of the car floor where the center of the car floor moves up and down. The car floor fixing was also tested in practice by fixing it with an angle bracket to the car frame showing good response in reducing the resonances amplitudes.

Considering the results of the case studies it can be said that the meshless method implemented by SimSolid can be utilized for the ride quality analysis of the elevator car system. The SimSolid offers faster method for overall analysis process compared to traditionally used element method. The SimSolid can reduce the analysis time due two critical steps in FEM. The structure does not require any pre-processing or discretization as the 3D model of the systems assembly can be utilized as it is. Second step that reduces the analysis time is that SimSolid does not require mesh generated by the user. The meshless method allows any arbitrary piece of the structure become an element for example part of the assembly can be considered as one element. In the meshless method the shape functions estimating the structural deformations are based on the point scatter inside these elements. This way the elementwise discretization is performed automatically during the software's solving rung. This feature makes the meshless approach faster. The SimSolid dynamic analysis also was benchmarked against other available methods in this thesis. The benchmarking was done by performing a dynamic modal analysis for beam and plate structures. The results were compared to similar analysis done with FEMAP and some closed-form solutions found in the literature. The SimSolid's meshless method was proven to be equally capable of performing the analysis as the FEMAP's mesh based FEM for this type of analysis.

As an outcome from the case studies, the proposal for improving the ride quality was to adjust the car floor assembly. Instead of having the car floor resting on the car frame beam it should be fixed by gluing it to the beam. This way, the structure is tuned to reduce the amplitudes caused the forced vibrations. The method for damping the resonances by adjusting the properties of the isolation or its design were not studied in this thesis. The car systems structure includes Cellasto pads that isolate the excitations from the ropes and pulley

beams towards the car structure and ultimately to the car floor. Furtherly the isolation and damping design should be studied to improve the elevator car's ride quality.

References

Altair. 2021. Designer Oriented Software - Is it Accurate?. [Web document]. [Referred 10.10.2021]. Available in PDF-file: https://www.altair.com/resource/nafems-simsolid-benchmark

Altair. 2021. Altair SimSolid Technology Overview. [Web document]. [Referred 23.9.2021]. Available in PDF-file: https://www.altair.com/resource/altair-simsolid-technology-overview

Belytschko, T., Krongauz, Y., Organ D., Fleming, M., Krysl P. 1996. Meshless methods: And overview and recent developments. Computational methods in applied mechanics and engineering. Comput. Methods Appl. Mech. Engrg. 139 1996. Pp. 3-47

Belytschko, T., Duan, Q., Gao, X., Li X,.Wang B., Zhang, H. 2014. Consistent element-free Galerkin method. International Journal for Numerical Methods in Engineering. Published online 7.5.2014. Int. J. Numer. Meth. Engng 2014. Pp.79–101.

Blevins, R. D. 2016. Formulas for dynamics, acoustics and vibration. First edition. John Wiley & Sons, LTD. Pp. 137-216.

Braun, S. Ewins D. Rao S. 2002. Encyclopedia of Vibration, Volumes 1-3. Elsevier. Pp. 1290-1293.

BASF. 2021. Cellasto A cellural polyurethane elastomer [web document]. [Referred 02.01.2022] Available: https://furniture-wood.basf.com/global/Cellasto_cellular_en.pdf

Debney P. 2020. Computational Engineering. The Institution of Structural Engineers. Pp. 48.

Herrera, I. & Kaczmarczyk S. 2009. The assessment of vibration absorption capacity of elevator's passengers. 7th International Conference on Modern Practice in Stress and Vibration Analysis. Journal of Physics: Conference Series 181. Pp. 1-10.

Hitachi. 2017. New Globally Standardized Machine-room-less Elevator. [web document]. [Referred 2.10.2021]. Available:

https://www.hitachi.com/rev/archive/2017/r2017_03/08/index.html

Howkins R. 2006. Elevator Ride Quality - The Human Ride Experience. Elevcon 2006, Elevator Technology 16, Helsinki, Finland 2006. Pp. 9-638.

Inman, D. 2013. Engineering Vibration. 2013. Fourth edition. Pearson.

ISO18738.2012. Measurement of Ride Quality part1: lifts (elevators).ISO. 5 p. Confirmed and published in English.

KONE. 2021. [Web Page]. https://www.kone.fi/referenssit-ja-tarinat/artikkelit/lisatilaa-vuodesta-1996.aspx

Kurowski, P. 2004. Finite Element Analysis for Design Engineers. First Edition. SAE INTERNATIONAL. Warrendale, Pennsylvania, USA. Pp. 89-111.

Kurowski, P. 2017. Finite Element Analysis for Design Engineers. Second Edition. SAE INTERNATIONAL. Warrendale, Pennsylvania, USA. Pp. 185-186.

Li, K., Suen, A., Wu, E., 2004. A General Survey on Lift Ride Quality at Public Building of the Honk Kong Special Administrative Region. CBTUH 2004 Seoul Conference. Pp. 69-75.

Liu, G.R. 2010. Meshfree Methods Moving Beyond the Finite Element Method. Second edition. CRC Press. Pp. 21-705.

Liu, G.R. Gu, Y.T. 2005. An Introduction to Meshfree Methods and Their Programming. Springer. Pp. 37-98.

Mac Donald, B. J. 2011. Practical Stress Analysis with Finite Elements. Second edition. Dublin. Glasnevin Publishing. Pp. 2-256

Mäkelä, M., Soininen S., Tuomola, S., Öistämö, J. 2012. Tekniikan Kaavasto. 2012 10th edition. Tammertekniikka / AMK-Kustannus Oy. Pp. 93.

Newland, D. 1989. Mechanical Vibration Analysis and Computation. Dover Publifications. Pp. 122-123.

Pavlou, D. 2015. Essentials of the Finite Element Method - For mechanical and Structural Engineers. Elsevier. Pp.2-35.

PVM. 2018. Elevator Ride Quality. [Web Document]. [Referred 16.11.2021]. Available: https://www.pmtvib.com/support.

Rao, S. 2018. Finite Element Method in Engineering. 6th edition. Elsevier. Pp. 84-458

Steinberg, D. 2000. Vibration Analysis for Electronic Equipment. 3rd edition. John Wiley & Sons. Pp. 63.

Szydło, K., Wolszczak, P., Longwic, R., Litak G., Dziubiński, M., Drozd, A. 2019. Assessment of Lift Passenger Comfort by the Hilbert–Huang Transform. Journal of Vibration Engineering & Technologies 8. Pp. 373–380.

Taylor, R., Zienkiewicz, O. 2000. Finite Element Method. 5th edition. Elsevier. Pp. 431-438.

Appendix 1. Results of modal analysis, benchmarking

Table 1. Natural frequencies of beam obtained from FEMAP and SimSolid analysis.

Mode	FEMAP [Hz]	SimSolid [Hz]
1	13.968	13.950
2	18.589	18.568
3	86.545	86.424
4	114.180	114.043
5	234.437	237.546
6	238.111	237.744
7	310.215	309.810
8	432.608	432.263
9	455.427	454.630
10	583.925	583.080
11	703.313	712.627
12	731.110	729.649
13	921.218	919.757
14	1056.404	1054.021
15	1172.192	1187.662
16	1297.094	1296.178
17	1307.875	1305.654
18	1423.028	1419.473
19	1641.075	1662.625
20	1732.11	1729.066

Table 2. Natural frequencies of clamped beam obtained from FEMAP and SimSolid analysis.

Mode	FEMAP [Hz]	SimSolid [Hz]
1	194.709	194.006
2	252.451	251.589
3	514.136	511.682
4	648.368	645.660
5	702.085	715.498
6	957.203	951.684

Table 2 continues. Natural frequencies of clamped beam obtained from FEMAP and SimSolid analysis.

Mode	FEMAP [Hz]	SimSolid [Hz]
7	1174.189	1168.727
8	1302.091	1300.537
9	1404.083	1431.483
10	1493.577	1483.823
11	1785.918	1777.317
12	2099.606	2084.854
13	2105.889	2147.951
14	2455.434	2444.001
15	2598.976	2597.006
16	2756.669	2736.732
17	2807.361	2864.555
18	3163.657	3150.406
19	3450.819	3426.206
20	3508.311	3581.227